View metadata, citation and similar papers at core.ac.uk
brought to you by CORE
provided by VCU Scholars Compass

Virginia Commonwealth University
VCU Scholars Compass

Theses and Dissertations Graduate School

2013

STRUCTURAL AND FUNCTIONAL CHARACTERIZATION OF SORTASE A

Vishaka Santosh
Virginia Commonwealth University

Follow this and additional works at: http://scholarscompass.vcu.edu/etd

Part of the Biochemistry, Biophysics, and Structural Biology Commons

© The Author

Downloaded from
http://scholarscompass.vcu.edu/etd/3051

This Thesis is brought to you for free and open access by the Graduate School at VCU Scholars Compass. It has been accepted for inclusion in Theses and Dissertations by an authorized administrator of VCU Scholars Compass. For more information, please contact libcompass@vcu.edu.

©Vishaka Santosh 2013
All Rights Reserved

STRUCTURAL AND FUNCTIONAL CHARACTERIZATION OF SORTASE A

A thesis submitted to the partial fulfillment of the requirements for the degree of Master of Science at Virginia Commonwealth University

Vishaka Santosh
Virginia Commonwealth University

Director: William A. Barton

Associate Professor, Department of Biochemistry and Molecular Biology

Virginia Commonwealth University
Richmond, Virginia
May 2013

ACKNOWLEDGMENTS

I would like to thank my family and friends for their emotional support through this intense process. I would also like to thank my advisor, Dr. William Barton, who offered my guidance and support throughout my studies.

TABLE OF CONTENTS

List of figures vi

List of abbreviations vii

Chapter 1: Introduction 1

1.1 Protein engineering 1

1.2 Protein ligation 2

1.3 Enzymatic protein ligation 8

1.4 Sortase 11

1.5 Sortase A 14

1.5.1 Structure of *S.aureus* SrtA 17

1.5.2 Kinetics of *S.aureus* SrtA 26

Chapter 2: Methods 32

2.1 DNA Cloning 32

2.2 Recombinant Protein Expression and Purification 32

2.3 Crystallization 32

2.4 Peptide synthesis 33

2.5 Kinetic assay 34

Chapter 3: Results 35

3.1 Sortase A expression and purification 35

3.2 Crystallization of Sortase A 38

3.2 Kinetics of pentaglycine substrate of Sortase A 50

Chapter 4: Conclusions 59

Literature Cited 73

List of Figures

Chapter 1: Introduction

Figure 1: Schematic representation of a ligation reaction……………………...4

Figure 2: Schematic representation of native chemical ligation..........................6

Figure 3: Schematic representation of subtiligase ligation..................................9

Table 1: List of all sortase families, their function and signal sequence...........12

Figure 4: Schematic representation of Sortase A reaction *in vivo*......................15

Figure 5: Overall fold of *S.aureus* Sortase A..18

Figure 6: Crystal structure of *S.aureus* SrtA bound to substrate. 20

Figure 7: NMR structure of *S.aureus* SrtA bound to substrate. 22

Figure 8: Surface model of *S.aureus* Sortase A with the Calcium binding residues highlighted 24

Figure 9: Schematic representation of the reverse protonation mechanism of *S.aureus* Sortase A..28

Figure 10: Surface model of *S.aureus* Sortase A in the “closed” conformation 30

Chapter 3: Results

Figure 1: 15% SDS Page gel of purified Sortases 36

Figure 2: *G.moribillorum* Sortase A crystal with respective diffraction patterns..40

Figure 3: Optimized *G.moribillorum* Sortase A crystals with respective diffraction patterns 42

Figure 4: 1.8Å structure of *G.moribillorum* Sortase A 44

Figure 5: Overlay of *G.morbillorum* Sortase A, apo *S.aureus* Sortase A and *S.aureus* Sortase A bound to LPAT..46

Figure 6: *L.bacterium* Sortase A crystal with repective diffraction pattern 48

Figure 7: Immunoblot of WT *S.aureus* Sortase A pentaglycine reaction...........51

Figure 8: Immunoblot of Liu’s *S.aureus* Sortase A pentaglycine reaction.........53

Figure 9: Immunoblot of Muna’s *S.aureus* Sortase A pentaglycine reaction.....55

Figure 10: Michaelis-Menten curve of pentaglycine kinetics of WT *S.aureus* Sortase A, Liu’s *S.aureus* Sortase A, and Muna’s *S.aureus* Sortase A...............................57

Chapter 4: Conclusions

Figure 1: Surface model of Muna’s *S.aureus* Sortase A mutations 63

Figure 2: Surface model of Liu’s *S.aureus* Sortase A mutations 65

Figure 3: BLAST sequence alignment of different Sortase A strains 67

Figure 4: Schematic representation of the pentaglycine assay 69

Table 1: Kinetic data on WT *S.aureus* Sortase A and mutants 71

List of Abbreviations

NHS	N-hydroxysuccinimidyl
PCR	Polymerase Chain Reaction
S.aureus	*Staphylococcus aureus*
MRSA	Methicillin Resistant Staphylococcus Aureus
ORF	Open Reading Frame
Nickle-NTA	Nickle-nitrilotriacetic acid
TFA	Triflouroacetic acid
TIS	Triisopropylsilane
HPLC	High Pressure Liquid Chromatography
MALDI-TOF	Matrix Assisted Laser Desorption Ionization-Time of Flight
YFP	Yellow Flourescent Protein
BME	β-mercaptoethanol
PVDF	Polyvinylidene fluoride
HRP	Horseradish peroxidase
TBST	Tris Buffer Saline Tween
G.moribillorium	*Gemella moribillorum*
L.bacterium	*Listeriaceae bacterium*
S.carnosus	*Staphylococcus carnosus*
L.mail	*Lactobacillus mali*

ABSTRACT

STRUCTURAL AND FUNCTIONAL CHARACTERIZATION OF SORTASE A

By Vishaka Santosh

Director: Dr. William A. Barton

Associate Professor, Department of Biochemistry and Molecular Biology

Sortases have been known to be essential in Gram-positive bacteria for attaching proteins onto the peptidoglycan layer of the bacterium. Sortase A has been found to be useful as a “molecular stapler”, although; in vivo, the enzyme is responsible for attaching proteins to the peptidoglycan layer of Gram-positive bacteria. It accomplishes both of these tasks by joining two proteins together via an LPXTG sorting sequence. The enzyme has been proven to be very useful in attaching any two proteins together without worrying about recombinant techniques to generate the fusion protein. The problem with this enzyme is that the catalytic diad, which is composed of Cys-184 and His-120, has to be in a certain form that exists .2% of the time at pH 7.0. There is also a hydrolytic shunt that the enzyme can undergo instead of the productive transpeptidase reaction. These issues lead to groups attempting to place *S.aureus* SrtA through directed evolution in order to increase the catalytic efficiency of the enzyme. Although mutants have been generated that increase the catalytic efficiency 13-fold and 130-fold, the structural basis behind this increase is poorly understood. Using crystallography, we will attempt to discover the structural basis behind the rate enhancement as well as understand more about

different species of SrtA. We also will attempt to kinetically characterize the *S.aureus* SrtA enzyme, its mutants, and different strains of SrtA. Thus far *G.moribillorum* SrtA has been crystallized and its structure shows that there is a distinction in the β6/β7 loop which has been implied to be important to catalysis. Furthermore, the pentaglycine kinetics shone some light on how the different mutants interact with the pentaglycine substrate of *S.aureus* SrtA.

Chapter 1

Introduction

1.1 Protein engineering

As of February 2012, the Protein Data Bank reports that there are 88512 structures that have been solved (*Protein Data Bank,* 2012). Adding to that accomplishment is the fact that 4169 genomes have also been sequenced (*Genomes Online Database*, 2012). Despite these achievements, the biological function of many of these proteins with known structure and sequence has yet to be elucidated. Most current "function predicting" algorithms rely on sequence and structural alignment, although these methods often fail to yield definitive answers (David Lee et. al, 2007). For example, homologous proteins might have different functions even though they are structurally and genetically very similar. In light of this problem, protein engineering has undergone resurgence as an approach that can be used in order to better understand the function of these orphan proteins (James C. Whisstock et. al, 2003).

Protein engineering is the process by which a protein is altered so that it's properties may be improved for various different applications. Through this method, it is possible to alter the framework of the protein and understand how each piece of the framework contributes to the protein's function (Romas J. Kazulaskas et. al, 2009). The ability to engineer a protein depends on the amount of information that is available on said protein. If a lot of information is known about a protein, a more "rational" approach is implemented. This approach uses what information is known about the protein and employs methods such as molecular modeling, to determine new characteristics. In the case where not a lot of information is known on the protein, a "directed evolution" approach is employed. This tactic uses techniques such as mutagenesis and error-prone PCR to randomly generate mutations. These mutated proteins are placed through a selection process and the most ideal combination of mutations is chosen. Relying entirely either on a rational or directed evolution approach is not the most ideal, so a combination of the two methodologies is the best. A structure based evolution strategy uses the known structure of the protein and mutates residues on domains in order to see what impact it has on the function (Peter Kast et. al, 1997).

1.2 Protein ligation

In order to generate an altered protein, modifications are required that, at times, are difficult to implement via typical recombinant methods. In order to circumvent these issues, protein fusion and protein ligation methods have been developed.

Protein ligation is a tool by which one can selectively join two peptides or proteins together. This method can allow for the incorporation of flourophores, unnatural amino acids, or other probes to the peptide or protein (Figure 1.1). The two methods of ligation are chemical and enzymatic ligation. Two main examples of chemical ligation techniques are native chemical ligation and targeted chemical modifications towards cysteines and lysines. Although both of these methods have been useful, each of them comes with their own set of problems. Native chemical ligation uses unprotected peptides with an N-terminal cysteine on the carboxy-terminal peptide and a C-terminal thioester on the other amino-terminal peptide. The N-terminal cysteine attacks the C-terminal thioester resulting in a trans-thioesterification reaction. The intermediate formed in this reaction rearranges via an N,S acyl shift which results in the two peptides joined together via a native peptide bond (Nathalie Olliver et. al, 2010, Figure 1.2). One concern with this method is that there is a size limitation on the peptide substrates and the reaction is rather slow. The other example of chemical ligation comes from directly labeling cystines and lysines. Malemides and N-hydroxysuccinimidyl (NHS) esters have been used in order to accomplish this task though it generally lacks the specificity that is sometimes required to generate fusion proteins. The limitations of size and specificity from chemical ligation lead to the use of enzymes to conduct the ligation reactions.

Figure 1.1: A ligation reaction requires a free carboxylic acid group and a free amine group. The carboxylic acid group-containing moiety (green) reacts with an amine-containing moiety (blue) to form water and a ligated product.

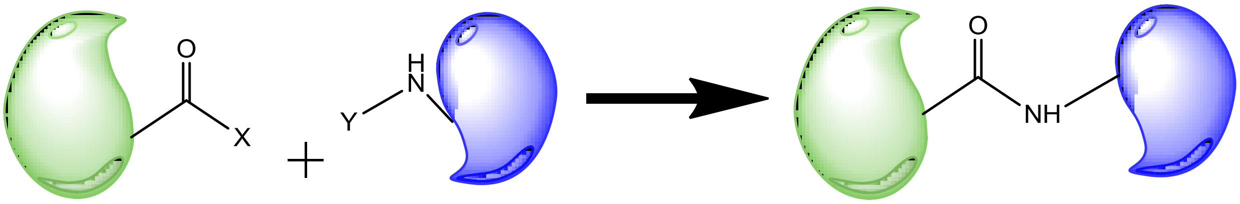
O
X
Y
H
N
O
NH

Figure 1.2: Native chemical ligation requires the use of two reactive peptides. One peptide must have a C-terminal thioester (red) while another retains a reactive thiolate group such as an N-terminal cysteine (blue). The N-terminal cysteine residue attacks the C-terminal thioester followed by a transthioesterification. Following this step, an N-S acyl shift occurs which results in the formation of a fusion peptide.

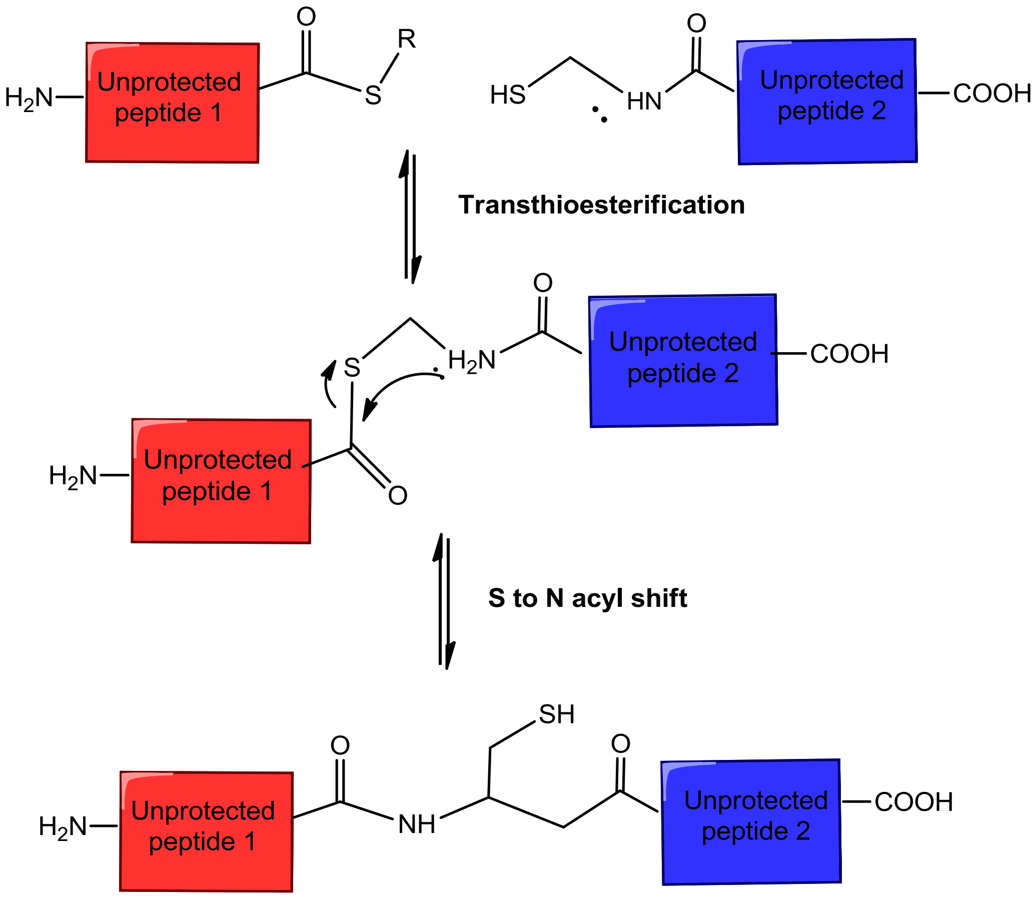
H2N
Unprotected peptide 1
O
R
S
HS
HN
O
Unprotected peptide 2
COOH
Transthioesterification
S
H2N
O
Unprotected peptide 2
COOH
H2N
Unprotected peptide 1
O
S to N acyl shift
SH
O
O
H2N
Unprotected peptide 1
NH
Unprotected peptide 2
COOH

1.3 Enzymatic protein ligation

Enzymatic protein ligation typically involves the recombinant insertion of a signal sequence (from six to thirty-eight residues) that is recognized by the ligase. A well-known example capable of protein ligation is the engineered subtiligase. Subtiligase was originally engineered from subtilisin, a non-specific serine endopeptidase (Thomas K. Chang et.al, 1994). The subtiligase reaction consists of two main steps. The first step involves the use of an amine protected donor peptide to react with a deprotected acceptor peptide. Subtiligase attacks the donor peptides' ester to produce a thio-acyl intermediate. The acceptor peptides amine attacks the thio-acyl group on subtiligase to resolve the intermediate and release free enzyme. The final step removes the protecting group off the donor peptide to generate a free fusion peptide (David Y.Jackson et.al, 1994, Figure 1.3). Although subtiligase can be effective under some conditions, the intense step-wise esterification and ligation leads it be a cumbersome protein ligator.

An alternative to subtiligase is *Staphylococcus aureus* (*S.aureus*) Sortase A (SrtA) which has many of the benefits and few of the limitations.

Figure 1.3: A subtiligase reaction requires a donor and acceptor peptide. The donor peptide is shown in purple while the acceptor peptide is shown in teal. Subtiligase conducts the first ligation reaction while the deprotection of the donor peptide is accomplished with Zn and CH_3CO_2H.

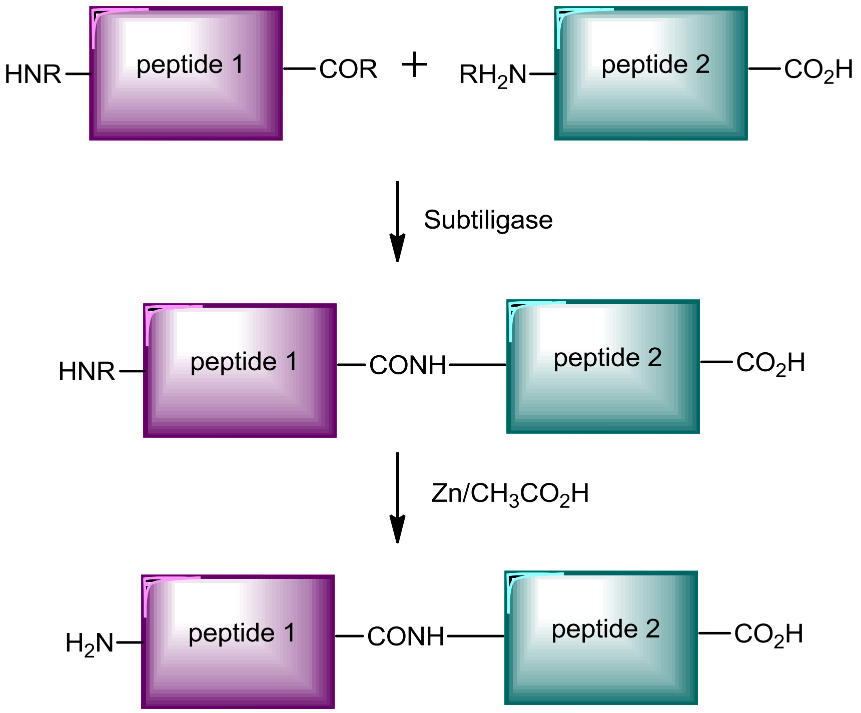
HNR
peptide 1
COR
+
RH2N
peptide 2
CO2H
Subtiligase
HNR
peptide 1
CONH
peptide 2
CO2H
Zn/CH3CO2H
H2N
peptide 1
CONH
peptide 2
CO2H

1.4 Sortase

Sortases are enzymes that are found ubiquitously in gram-positive bacteria and are essential for the incorporation of extracellular proteins into the peptidoglycan layer. There 4 sortase families: Sortase A, Sortase B, Sortase C, and Sortase D (Table 1.1, Hendrickx et. al, 2011). Each sortase family appears to perform a unique role in bacterial physiology. For example, Sortase B is responsible for attaching iron binding proteins to the peptidoglycan layer for iron scavenging. Unlike most of the sortases, Sortase B recognizes the Asparagine-Proline-Glutamine-Threonine-Asparagine (NPQTN) substrate motif and it attaches the proteins to the peptidoglycan crossbridge itself. Sortase C is involved with pilin synthesis and its substrate recognition motif is Leucine-Proline-X-Threonine-Glycine (LPXTG) where X represents any amino acid. Unlike the other sortase families, sortase C couples its substrate onto the side chain lysine residue within pilins. Sortase D is linked exclusively with spore formation. Its substrate recognition motif is Leucine-Proline-Asparagine-Threonine-Alanine (LPNTA) and the sortase D altered protein gets attached onto Lipid II which is a component of the peptidoglycan layer.

Table 1.1: There are four different types of sortases all of which have a distinct function.

The substrates, recognition motifs, and anchors are detailed below.

Sortase class	**Substrates**	**Substrate motif**	**Nucleophile**
Sortase A (SrtA)	Surface protein	LPXTG	Lipid II
Sortase B (SrtB)	Heme transport factor	NPQTN	Peptidogylcan crossbridge
Sortase C (SrtC)	Pilin proteins	LPXTG	Lys residue of pilins
Sortase D (SrtD)	Mother cell and endospore envelope proteins	LPNTA	Lipid II

1.5 Sortase A

Sortase A has been the focus of most research because of its use as an enzymatic protein ligator. In Gram-positive bacteria, SrtA is known as the “housekeeping sortase” because it is responsible for attaching various secreted proteins onto Lipid II via the signal sequence LPXTG where X is any amino acid (Figure 1.4). Some of the proteins that SrtA attaches to the peptidoglycan layer are involved in immune evasion and nutrient transport; because of the important role that SrtA plays in the utility of these proteins, it is an important virulence factor (Anthony W. Maresso et.al, 2008).

Figure 1.4: *In vivo,* SrtA attaches secreted proteins to the lipid bilayer of Gram positive bacteria. SrtA (in red) is anchored to the lipid bilayer of the cell membrane through its amino-terminal hydrophobic transmembrane domain. Secreted proteins containing the sorting signal LPXTG, are recognized by SrtA and anchored to the pentaglycine-bearing Lipid II prior to incorporation into the cell wall.

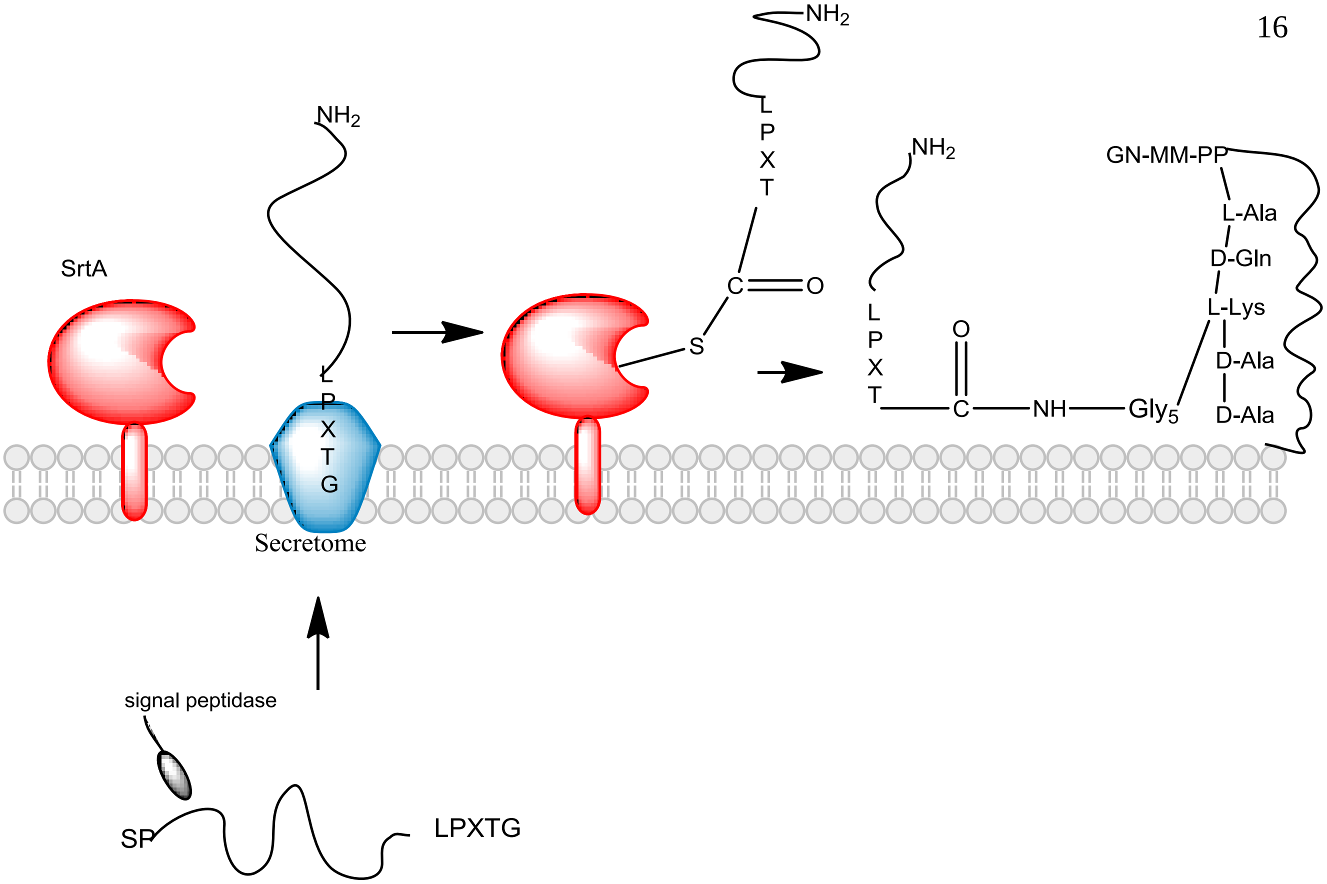
NH2
L
P
X
T
C
O
S
NH2
GN-MM-PP
L-Ala
D-Gln
L-Lys
D-Ala
D-Ala
SrtA
NH2
L
P
X
T
G
L
P
X
T
O
C
NH
Gly5
Secretome
signal peptidase
SP
LPXTG

1.5.1 Structure of *S.aureus* Sortase A

S.aureus SrtA is a 206 residue transpeptidase which consists of an N-terminal membrane spanning region and a C-terminal catalytic domain. The overall fold of the protein consists of a β-barrel structure containing eight alternating β-strands that seem to be unique to *S.aureus* SrtA (Udayar Ilangovan et.al, 2001, Figure 1.5). There are currently two structures of the active *S.aureus* SrtA. In the crystal structure, the LPXTG sorting signal binds in a “L” shaped conformation in the β6/β7 loop (Yinong Zhong et.al, 2007, Figure 1.6). The sorting signal is 8Å away from the active site (His120, Cys184) and the active site residues are 5Å away from each other. In the NMR model, the sorting signal binds in nonlinear conformation in the β6/β7 loop and the sorting signal is significantly closer to the active site (Nuttee Suree et.al, 2009, Figure 1.7). There is a 10Å difference in the β6/β7 loop between the crystal and NMR structure (Nuttee Suree et.al, 2009).

The calcium ion contributes to *S.aureus* SrtA activity by holding the β6/β7 loop in a steady conformation for optimal sorting signal binding (Mandar T. Naik et.al, 2005, Figure 1.8).

Figure 1.5: The overall structure of SrtA consists of a unique β-barrel fold. The blue represents the β-strands while the red represents the helices present in the protein. The N-terminus and C-terminus are labeled as well.

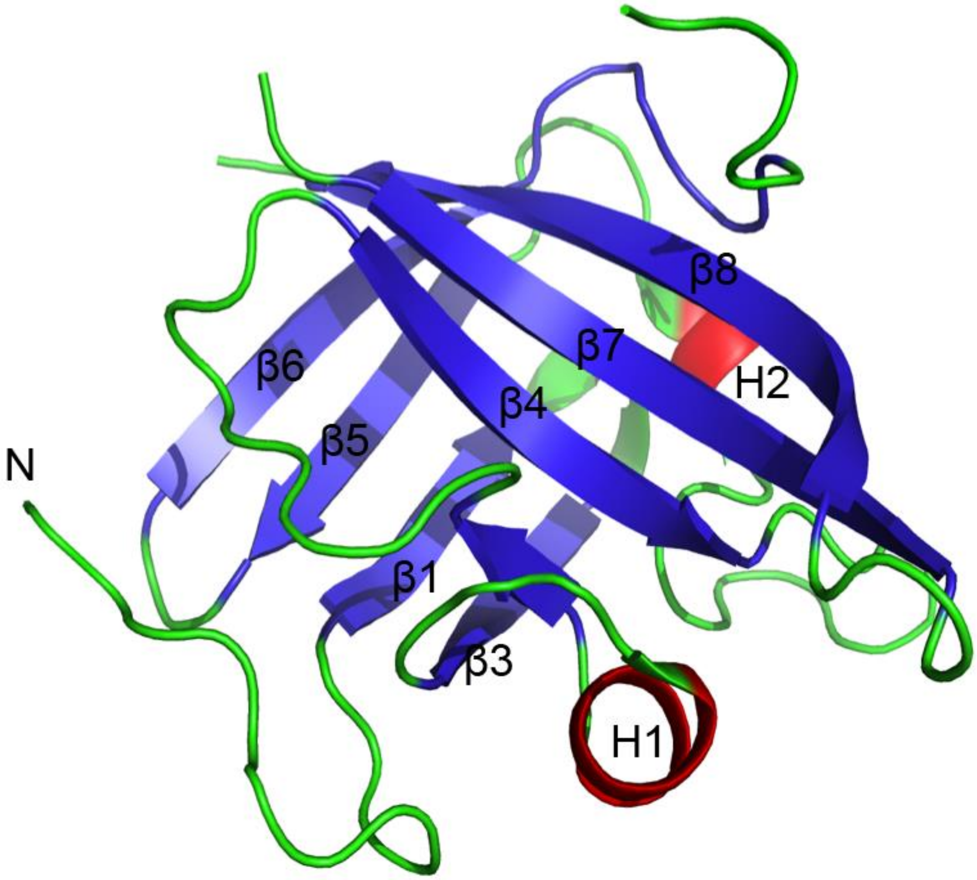
β8
β7
H2
β6
β4
β5
N
β1
β3
H1

Figure 1.6: Crystal structure of *S.aureus* SrtA bound to substrate. Overall surface of the enzyme is shown in cyan. The active site residues are labeled and are colored in red. The LPETG peptide is colored orange.

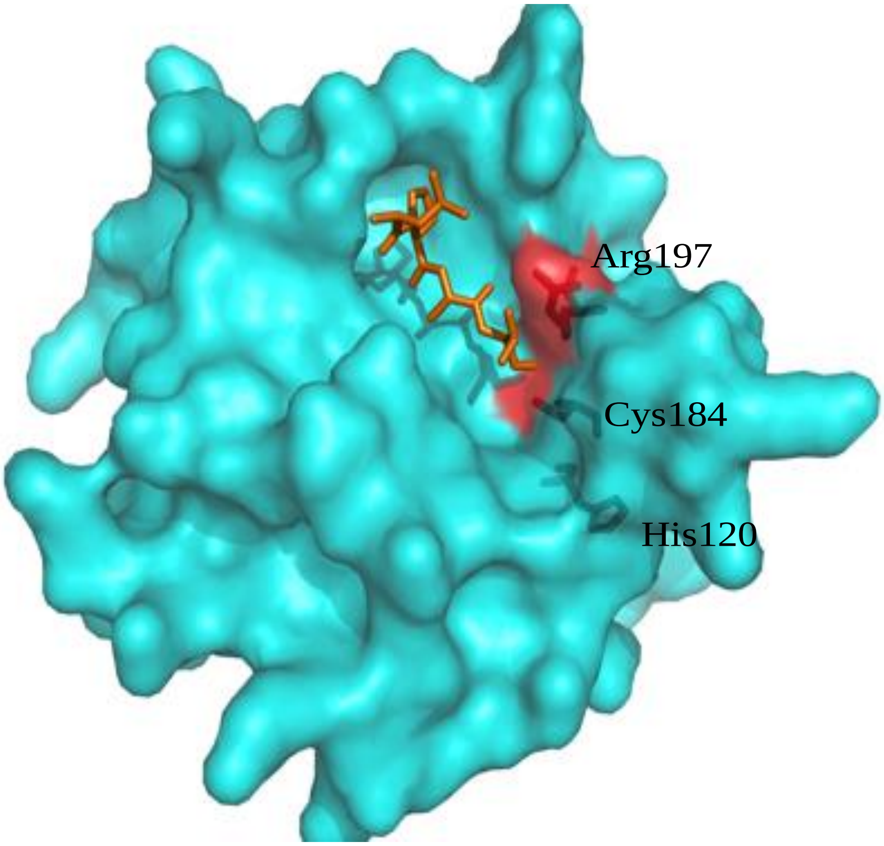
Arg197
Cys184
His120

Figure 1.7: NMR structure of *S.aureus* SrtA bound to substrate. The overall fold of the enzyme is given in cyan with the active sites labeled and colored in red. The LPETG peptide is colored orange.

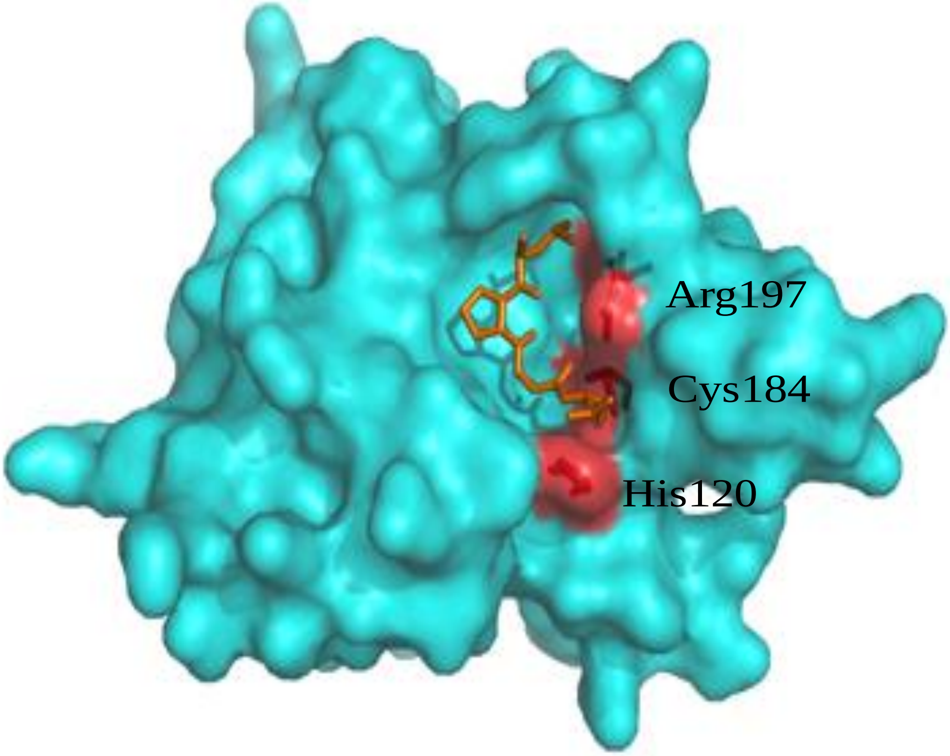
Arg197
Cys184
His120

Figure 1.8: Calcium binding stablizes the β6/β7 loop in *S.aureus* SrtA. The left picture shows the crystal structure of *S.aureus* SrtA with the calcium residues labeled while the right picture shows the NMR structure of *S.aureus* SrtA. In both pictures, the β6/β7 loop is colored in blue and the calcium binding helps hold the loop in a stable conformation for catalysis (as seen in the NMR model).

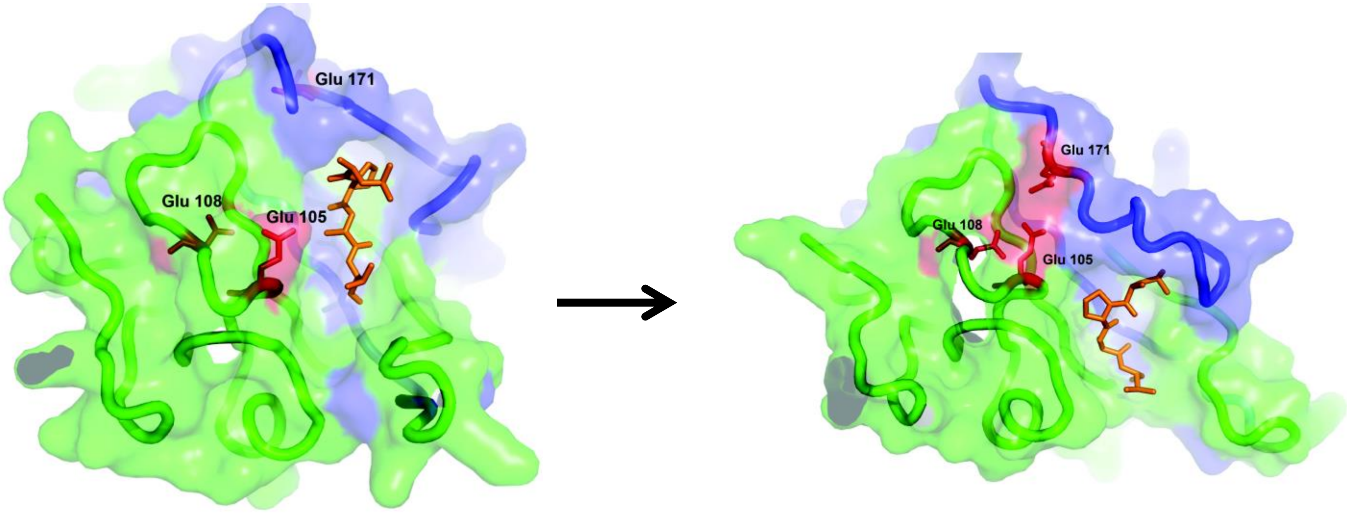
Glu 171
Glu 108
Glu 105
Glu 171
Glu 108
Glu 105

1.5.2 Kinetics of *S.aureus* Sortase A

The catalytic triad of *S.aureus* Srt A is composed of Histidine-120, Cysteine-184, and Arginine-197. Sortase A uses a reverse-protonation reaction mechanism in which Cysteine-184 and Histidine-120 act as a thiolate-imidazolium ion pair during catalysis (Hung Ton-That et.al, 2002; Brenda A. Frankel et.al, 2005). The Cysteine-184 thiolate attacks the carbonyl group between the Threonine and Glycine in the signal sequence forming a tetrahedral intermediate. Histidine-120 is then deprotonated by the amide group between the Threonine and Glycine which leads to the formation of a thio-acyl intermediate. Histidine-120 abstracts a proton from the pentaglycine amide group which allows the pentaglycine group to attack the thioacyl intermediate. This leads to a tetrahedral intermediate which is rearranged to faciliate the release of Cystine-184 and the newly formed peptide (Brenda A. Frankel et.al, 2005, Figure 1.9). The role of Arginine-197 is debated, but the most current molecular dynamics simulations imply that Arginine-197 is necessary for substrate binding (Bo-Xue Tian et.al, 2011). Recent NMR studies show that it does not stabilize the catalytic diad (Nuttee Suree et.al, 2009).

Although the mechanism seems to be straightforward, several problems arise when *S.aureus* SrtA is used for protein ligation. As stated previously, the enzyme is active when Cystine-184 is in its thiolate form and Histidine-120 is in its imidazolium form suggesting that at pH 7 only .2% of the enzyme is in the active form. Futhermore *S.aureus* SrtA can utilize an unproductive hydrolytic shunt which decreases the overall yield (Brenda A.Frankel et.al, 2005, Figure 1.10). Both issues limit the enzyme's catalytic efficiency ($k_{cat}/K_m = 125 \pm 18\ M^{-1}s^{-1}$ (Matthew L.Bentley et.al, 2008)). There are several different solutions that have been used to overcome the kinetic obstacles of

S.aureus SrtA. For example, it is not uncommon to see SrtA used in stoichiometric amounts during ligation reactions Similarly, one group reported the usage of a β-hairpin loop near the signal sequence so the enzyme could not use the hydrolytic shunt due to steric hindrance (Yuichi Yamamura et.al, 2010). Alternatively, Chen et.al explored the possibility of directed evolution to increase its catalytic activity. They were able to generate a mutant that has a 100-fold increase in the catalytic efficiency (Irwin Chen et.al, 2011),

Figure 1.9: The reverse protonation mechanism of SrtA is unique and involved. Each step is detailed down below and the red Roman numerals indicate the step of the reaction.

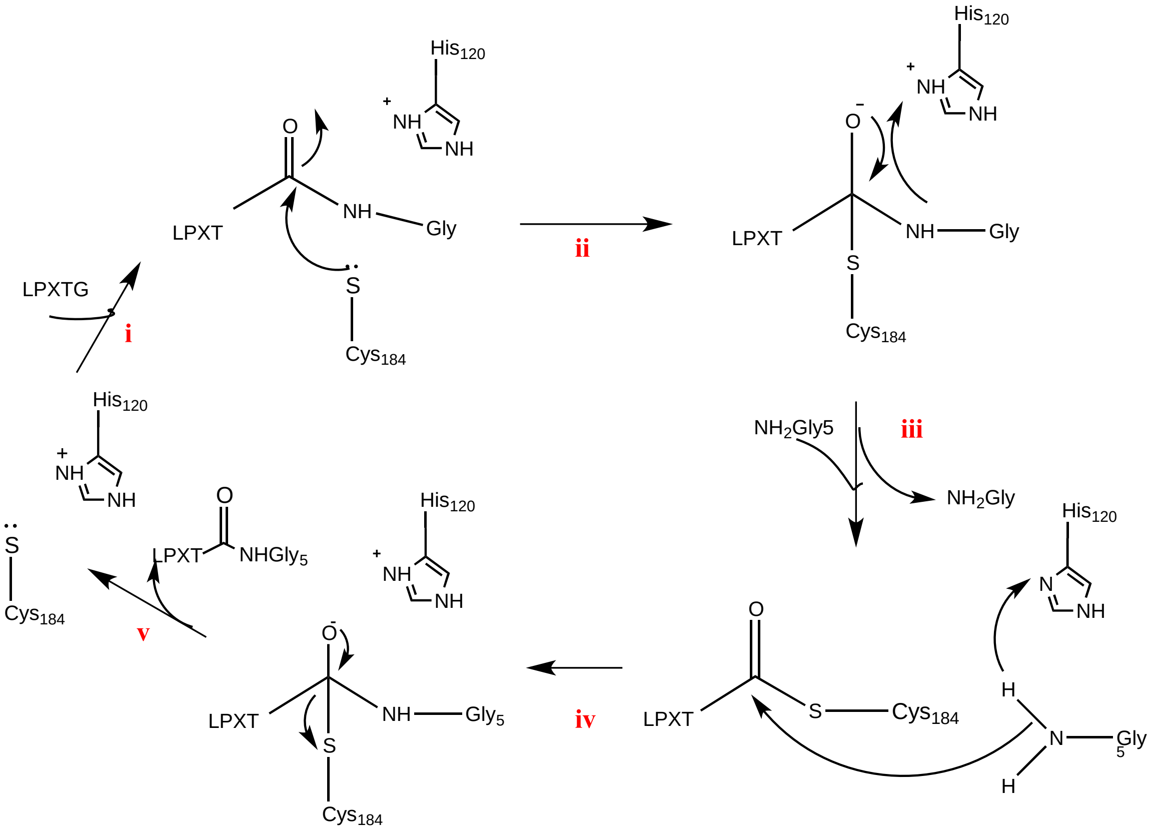

His120
NH
NH
O
LPXT
NH
Gly
S
Cys184
LPXTG
i
ii
O
LPXT
NH
Gly
S
Cys184
iii
NH2Gly5
NH2Gly
O
LPXT
S
Cys184
H
N
Gly5
H
N
NH
iv
O
LPXT
NH
Gly5
S
Cys184
v
O
LPXT
NHGly5
S
Cys184

Figure 1.10: The SrtA transpeptidation is a ping pong ordered bi bi reaction while the hydrolytic shunt a ping pong bi uni reaction. The enzyme can either undergo the hydrolysis reaction or the productive transpeptidation reaction depending on the availability of a productive nucleophile.

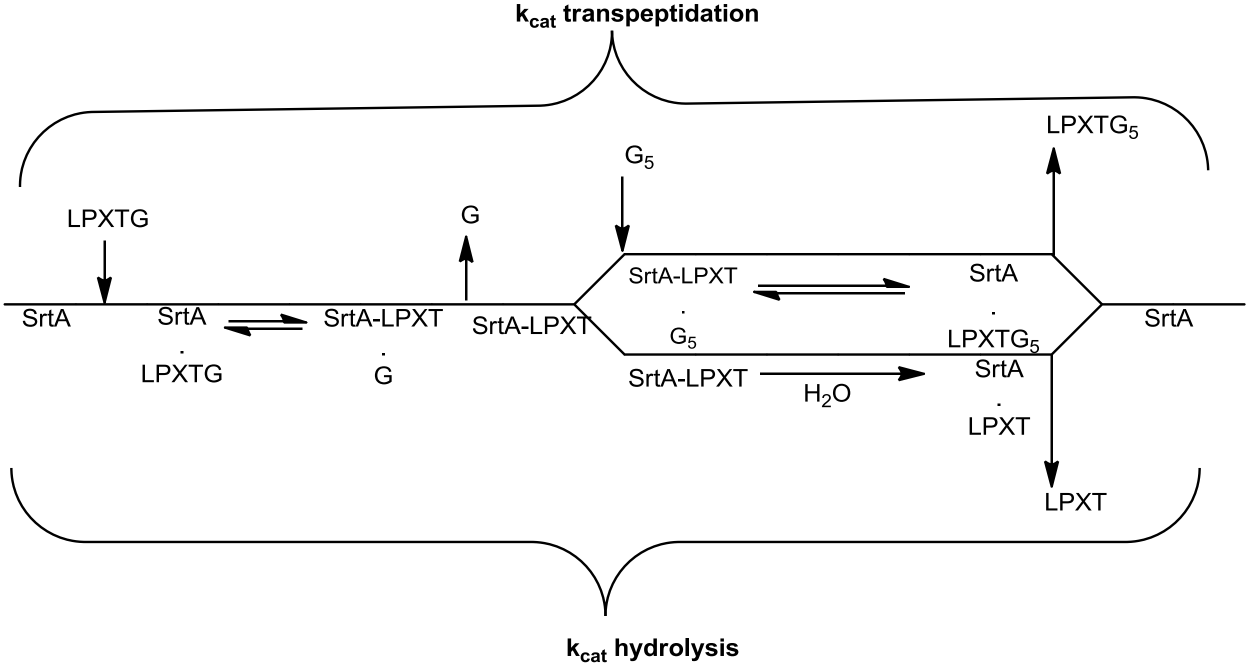
k_{cat} transpeptidation
LPXTG
SrtA
SrtA · LPXTG
SrtA-LPXT · G
G
SrtA-LPXT
G_5
SrtA-LPXT · G_5
SrtA · $LPXTG_5$
$LPXTG_5$
SrtA
SrtA-LPXT
H_2O
SrtA · LPXT
LPXT
k_{cat} hydrolysis

Chapter 2

Methods

2.1 DNA Cloning

All of the SrtA strain and mutant sequences were codon-optimized for E-coli expression and synthesized by Gene Script. Each open reading frame (ORF) was subcloned into pET28 expression vectors (Novagen) to be expressed in *Escherichia coli* (*E.coli*) cells. For purification purposes, a hexa-histidine tag was added onto all of the N-termini of the protein.

2.2 Recombinant expression and purification

All constructs were transformed into BL21 *E.coli* and were grown using auto-induction media at 22-37^{o} Celsius overnight (F. William Studier, 2005). Following harvest, the cells were lysed in an Emulsifex C6 homogenizer at 20,000 psi. The lysate was clarified via a 60-minute spin at 20,000xg in a Ti45 rotor using a Beckman Coulter ultracentrifuge. The soluble fraction was run over a 20mL Nickle-NTA column that was washed with 20mM Tris-HCl pH 8.0, 300mM NaCl. Then, a specific elution profile was implemented. First, a five column-volume linear gradient with 50% of the elution buffer was implemented which was then followed by a 2 column-volume linear gradient to 100% of the elution buffer. The elution buffer was: 20mM Tris-HCl pH 8.0, 300mM NaCl, 200mM imidazole. Peak fractions were pooled, concentrated and run on a SD 75 gel filtration column in 20mM Tris-HCl pH 8.0, 300mM NaCl. Fractions were analyzed via SDS Page on a 15% acrylamide gel. After a clean peak was obtained from the gel filtration column, the peak was stored at -80^{o} Celsius upon the addition of 10% glycerol.

2.3 Crystallization

For crystallization, proteins were concentrated down to ~20mg/mL and buffer exchanged into 10mM bis-tris propane pH 7.0, 50mM NaCl. Initial crystallization conditions were identified using hanging-drop vapor diffusion on a 48-well plate using Hampton Research and Emerald Biosystems sparse matrix crystallization screens. The drop volume used was 2μL (1μL protein solution and 1μL mother liquor solution). The crystallization solutions used were Crystal Screen I and II (Hampton Research), Wizard Screen I and II (Emerald Biosystems), and Salt Screen I and II (Hampton Research). The trays were stored at 23^{o} Celsius.

2.4 Peptide synthesis

All peptides were prepared using manual solid-phase Fmoc chemistry on Rink-amide resin (Novagen;Young-Woo Kim et.al, 2011). Peptides were cleaved from the resin using a standard TFA cocktail which consisted of 95% TFA, 2.5% TIS and 2.5% water. Dried crude peptides were stored in 50% acetonitrile, 50% water at -80^{o} Celsius. Peptides were further purified via reverse phase HPLC (High Pressure Liquid Chromatography) on prep-grade C18 columns with a mobile phase of acetonitrile and 0.1% TFA. Some peptides were characterized via MALDI-TOF to confirm their composition and purity.

2.5 Kinetics assay

To determine the SrtA kinetic parameters for the pentaglycine substrate, an assay was developed to monitor the formation of biotinylated product via Western-blot. The concentration of SrtA was kept constant at 500nM and the concentration of Yellow

Fluorescent Protein (YFP)-LPETG was kept constant at 7.4µM. The concentration of the G_5YYK-biotin peptide was varied between 100µM and 1mM and the buffer used was 50mM Tris-HCl, 150mM NaCl, 5mM $CaCl_2$ pH 7.5. The final reaction volume was raised to 100 µL and was conducted at 37^o Celsius. Samples were removed at 0 minutes, 15 minutes, 30 minutes, and 45 minutes and were quenched with 4X sample dye with β-mercaptoethanol (BME). Samples were resolved on a 10% SDS gel prior to transfer to a polyvinylidene difluoride (PVDF) membrane. The gel was blocked for one hour with milk and probed with 1µg/mL of Streptavidin-HRP in TBST for an hour. After washing the membrane, developing solution was added and the blot was developed.

Chapter 3

Results

3.1 Sortase A expression and purification

G.moribillorum SrtA, *L.bacterium* SrtA, *S.carnosus* SrtA, *L.mali* SrtA, *S.aureus* SrtA, Muna's *S.aureus* SrtA, and Liu's *S.aureus* SrtA were expressed under the control of a T7 promoter in BL21 cells. Soluble expression at 37^{o} Celsius in autoinduction media was noted for all proteins with the exception of *S.carnosus* SrtA and *L.mali* SrtA. For these proteins, The *E.coli* was grown at lower temperatures using LB media and inducing with 1mM IPTG. Yields varied but were approximately 130 mgs of protein per liter of culture.

Cultures were harvested by centrifugation at 8000 rpm for 20 minutes. The pellet was resuspended in 30 mLs of buffer (20mM Tris pH 8.0, 300mM NaCl) per liter of culture. The cells were lysed by three passages at 20,000 psi using a homogenizer. Insoluble debris was removed via ultracentrifugation at 20,000 rpm for one hour. The soluble fraction was loaded over a Nickle-NTA affinity column (20mL column volume) and eluted with a two-step gradient in the elution buffer 20mM Tris pH 8.0, 300mM NaCl, 200mM imidazole.

The peak fraction from the Nickle-NTA affinity column was pooled, concentrated and loaded to an SD75 gel filtration column. The following proteins were successfully purified to homogeneity: *S.aureus* SrtA, Muna's *S.aureus* SrtA, Liu's *S.aureus* SrtA, *G.moribillorum* SrtA and, *L.bacterium* SrtA (Figure 3.1). SrtA purity typically exceeded 98% as confirmed by SDS-Page.

Figure 3.1: Samples were resolved on 15% polyacrylamide SDS denaturing gel to confirm purity. The gels were stained with Coomassie Brilliant Blue. Approximately ~10ug were loaded onto the gel. Liu’s *S.aureus* SrtA runs anomalously in comparison to the other *S.aureus* SrtA constructs.

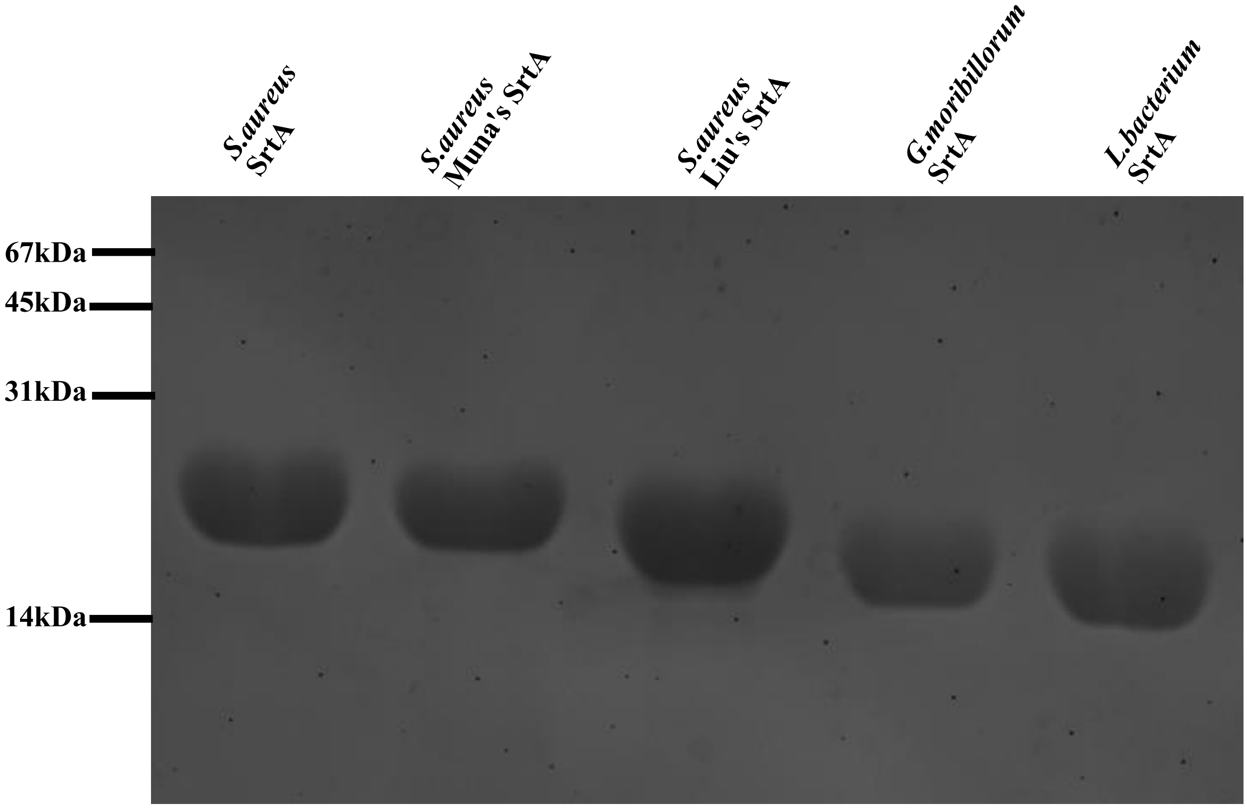
S.aureus SrtA
S.aureus Muna's SrtA
S.aureus Liu's SrtA
G.moribillorum SrtA
L.bacterium SrtA
67kDa
45kDa
31kDa
14kDa

3.2 Crystallization of Sortase A

For crystallization, pure SrtA proteins were concentrated down to ~20mg/mL and buffer exchanged with 10mM bis-tris propane, 50mM NaCl pH 7.0 and set against various sparse matrix screens via hanging-drop vapor diffusion on a 48-well plate. Initial hits were identified from Crystal Screen I and II (Hampton Research), and Wizard Screen I and II (Emerald Biosystems).

G.moribillorum SrtA initially crystallized in 60.0mg/mL in 2.0M Ammonium sulfate, .1M CAPS, .2M Lithium sulfate pH 10.5 at 23^{o}C. Several optimization screens were set up, and the optimal mother liquor was 2.0M Ammonium sulfate. 50mM CAPS, 30% 1,8-diaminooctane pH 10.4. This mother liquor yielded very large octahedral-like crystals that diffracted, but were very highly mosaic, so another set of crystallization conditions was attempted (Figure 3.2). *G.moribillorum* SrtA crystallized at 80.0mg/mL with the following mother liquors: 1.6M Ammonium sulfate, 50mM CAPS, pH 10.4, and 1.8.M Ammonium sulfate, 50mM CAPS, pH 10.4. Both solutions generated crystals that had a very similar morphological appearance to the initial *G.moribillorum* SrtA crystals (Figure 3.3). Data was collected at .98A on the 23-ID-D GM/CA-CAT beamline at Argonne National Labs. Two sets of data were obtained from the crystals; one set diffracted to 2.5Å and another set diffracted to 1.8Å. The space group of both crystals is $P4_32_12$. The phases were solved via molecular replacement with a side-chain truncated *S.aureus* SrtA structure as a search model. The 2.5Å data set produced a structure that did not have electron density for the β6/β7 loop, but the 1.8Å data set did have the needed electron density. The refined model for the 1.8Å structure has a R_{work} of 24% and a R_{free} of 26% (Figure 3.4). The *G.moribillorum* SrtA structure was structurally superimposed with *S.aureus* SrtA with and without the LPETG substrate (Figure 3.5). There is an rms deviation of 1.4Ǻ between the equivalent Cα atoms.

L.bacterium SrtA crystallized in 80.0mg/mL in 30% PEG 3000, .1M CHES pH 9.5 at 23°C. The crystals that arose from this solution were rods and formed a star-like structure (Figure 3.6). The crystals diffracted, but the diffraction pattern showed that there were multiple crystals in the line of the beam. Optimization screens were attempted on this condition, but no crystals grew. More crystallization conditions can be attempted by using microseeding, different temperatures, or different crystallization conditions.

S.aureus SrtA, Muna's *S.aureus* SrtA, and Liu's *S.aureus* SrtA were concentrated down to 100.0mg/mL, 60.0mg/mL and 20.0mg/mL respectively. Unfortunately, none of the proteins yielded crystals that could be analyzed. Liu's *S.aureus* SrtA yielded microcrystals in the following conditions: 20% PEG 1000 pH 7.0, 20% 1,4 butanediol pH 7.5, 2.0M Ammonium sulfate pH 7.0, 10% PEG 8000 pH 7.0, 1.5M Ammonium chloride pH 4.6, 1.8M Ammonium citrate pH 4.6, 3.5M Sodium formate pH 4.6, 1.5M Sodium nitrate pH 7.0, 1.0M Ammonium phosphate monobasic pH 4.6, 1.8M Sodium phosphate monobasic pH 7.0, and .5M Siccinic acid pH 7.0. In both Muna's *S.aureus* SrtA and Liu's *S.aureus* SrtA, a change in the crystallization buffer can be implemented to increase the concentration of the two proteins.

Figure 3.2: Initial *G.moribillorum* crystals were large but diffracted with high mosaicity. The crystals formed via hanging drop vapor diffusion in the mother liquor 2.0M Ammonium sulfate. 50mM CAPS, 30% 1,8-diaminooctane pH 10.4. The diffraction pattern of the crystals shows a high degree of mosaicity.

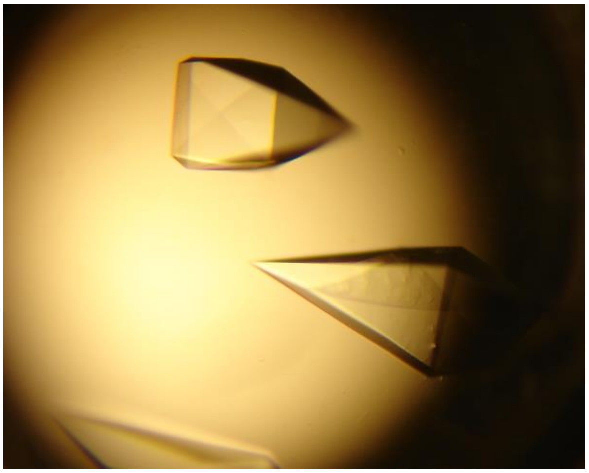

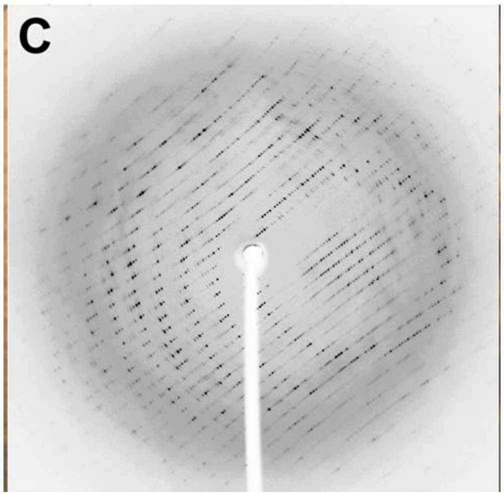
C

Figure 3.3: Optimized *G.moribillorum* crystals were large and diffracted to 1.8 Å. The crystals formed via hanging drop vapor diffusion in the following mother liquors: 1.6M Ammonium sulfate, 50mM CAPS, pH 10.4, and 1.8.M Ammonium sulfate, 50mM CAPS, pH 10.4.. The diffraction patterns of both crystals were fairly clear, but the second crystal did have some salt present in the diffraction pattern.

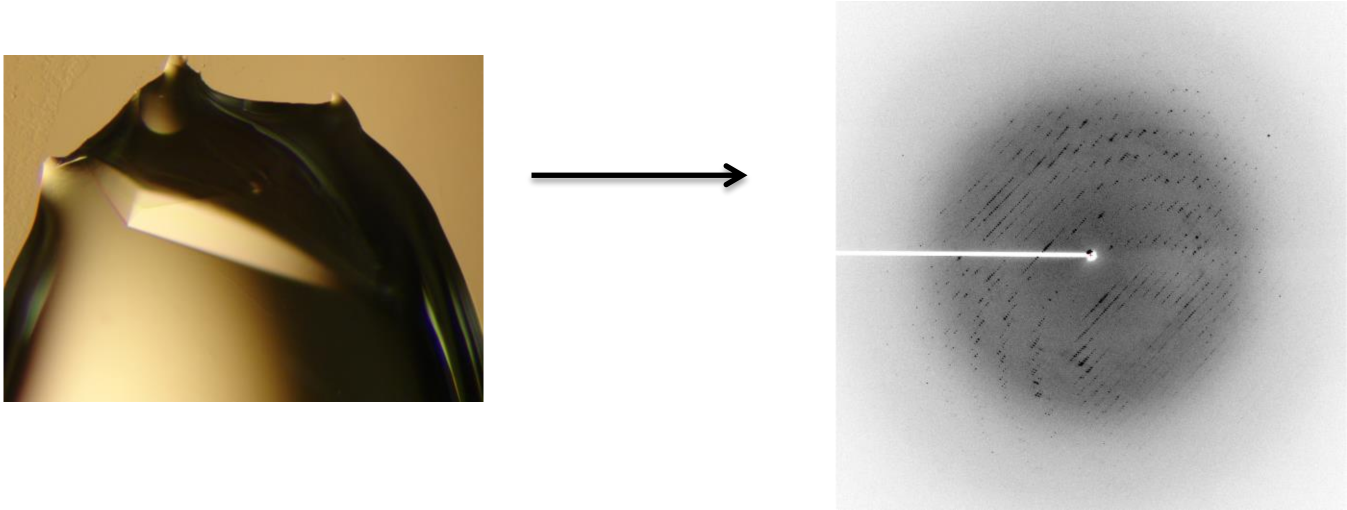

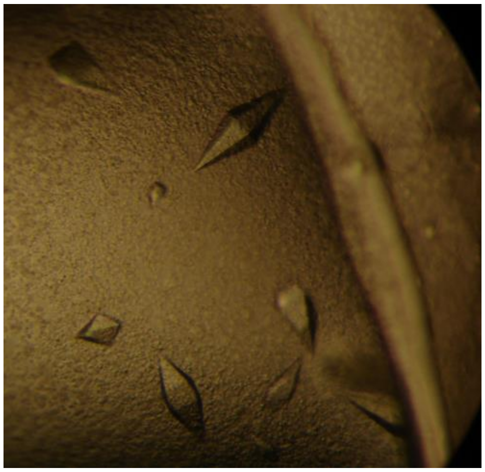

Figure 3.4: **1.8Å secondary structure of *G.moribillorum* SrtA.** The β6/β7 loop is colored in cyan while the β7/β8 loop is colored in green. The overall fold of the enzyme is colored in magenta.

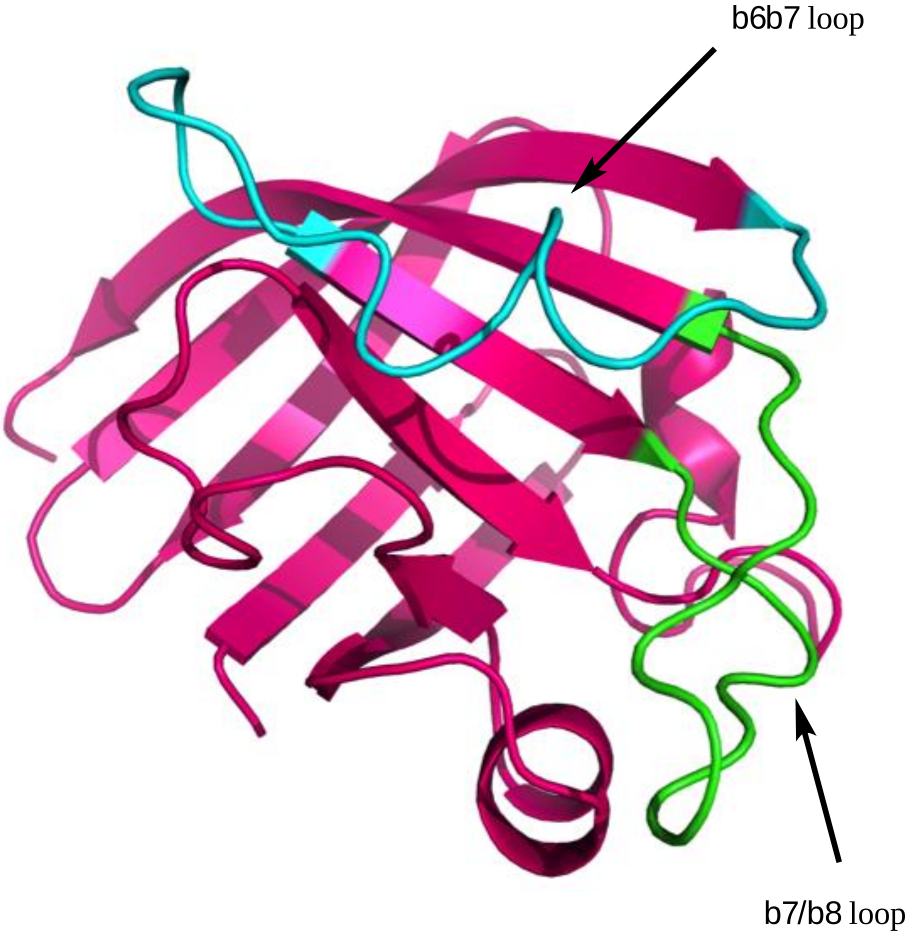
b6b7 loop
b7/b8 loop

Figure 3.5: G.moribillorum SrtA does not differ from S.aureus SrtA other than the differences in the β6/β7 loop. *G.morbillorum* SrtA is in magenta while *S.aureus* SrtA with LPETG and apo *S.aureus* SrtA are in green and purple respectively.

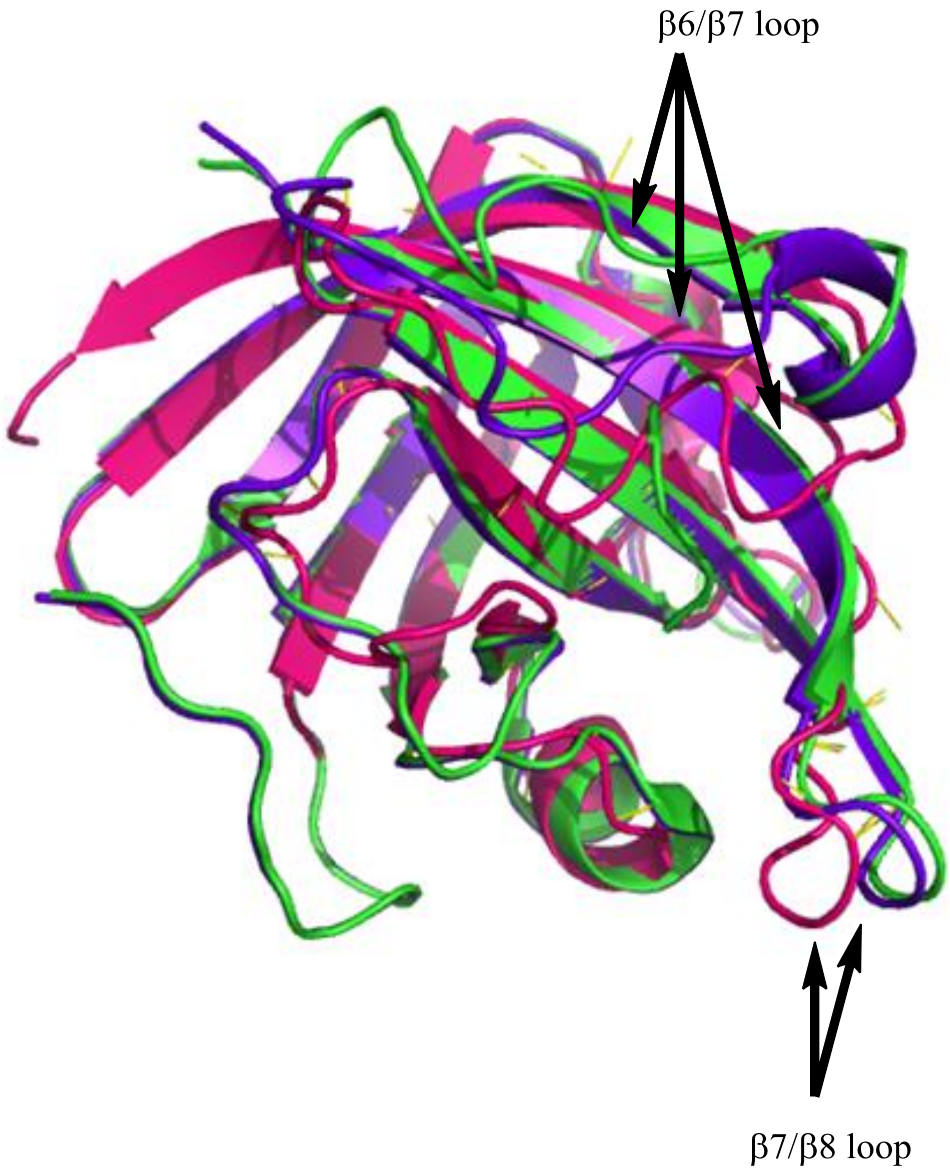
β6/β7 loop
β7/β8 loop

Figure 3.6: *L.bacterium* crystals formed, but diffracted with a high degree of heterogeneity. *L.bacterium* SrtA crystals formed out of the following mother liquor: 30% PEG 3000, .1M CHES pH 9.5.

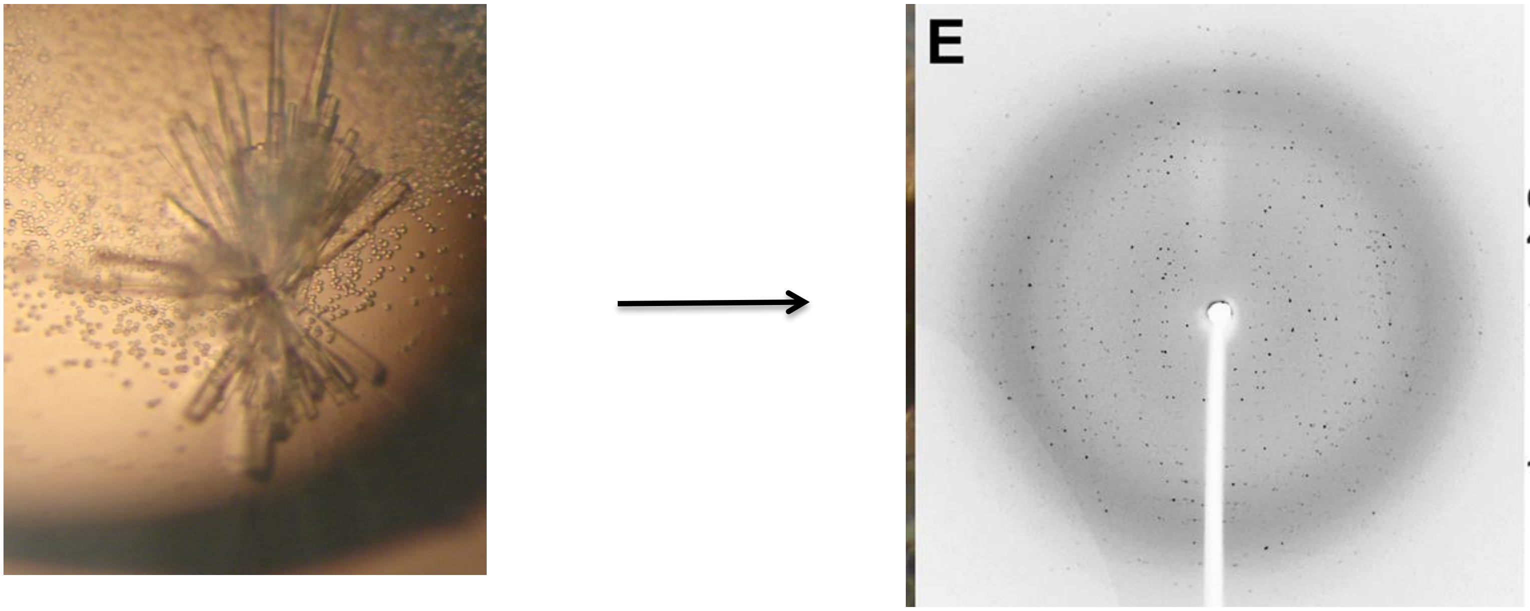
E

3.3 Kinetics of pentaglycine substrate of Sortase A

For kinetic analysis, we developed a Western-blot assay that could measure biotin incorporation into the final product. The concentration of sortase was kept constant at 500nM and the concentration of Yellow Fluorescent Protein (YFP)-LPETG was kept constant at 2mg/mL. The concentration of the G_5YYK-biotin peptide was varied between 100µM and 1mM. Samples were taken at 0 minutes, 15 minutes, 30 minutes, and 45 minutes and quenched with 4X sample dye containing β-mercaptoethanol (BME). Each time point was run on a 10% SDS gel and transferred to a PVDF membrane. After probing with Streptavidin-HRP in TBST for one hour, the blots were developed and analyzed via densitometry.

WT *S.aureus* SrtA was linear for all concentrations of the pentaglycine substrate for 0 to 15 minutes, but kinetic data could not be obtained because the Michaelis-Menten curve did not display a square hyperbolic shape and the rates were determined off two data points (Figure 3.7 and 3.9). Liu's *S.aureus* SrtA was also linear for all concentrations of the pentaglycine substrate for 0 to 15 minutes, and the Michaelis-Menten curve did display a square hyperbolic shape, but the rates were determined off two time points, so no kinetic data could be obtained (Figure 3.8 and 3.9). Muna's *S.aureus* SrtA displayed identical problems to WT *S.aureus* SrtA so no kinetic data could be obtained on Muna's *S.aureus* SrtA.

Figure 3.7: Western blot probing with streptavidin-HRP for YFP-G_5YYK_{biotin} using WT *S.aureus* SrtA. G_5YYK_{biotin} was titrated at the given concentrations and time points were taken at 15, 30, and 45 minutes.

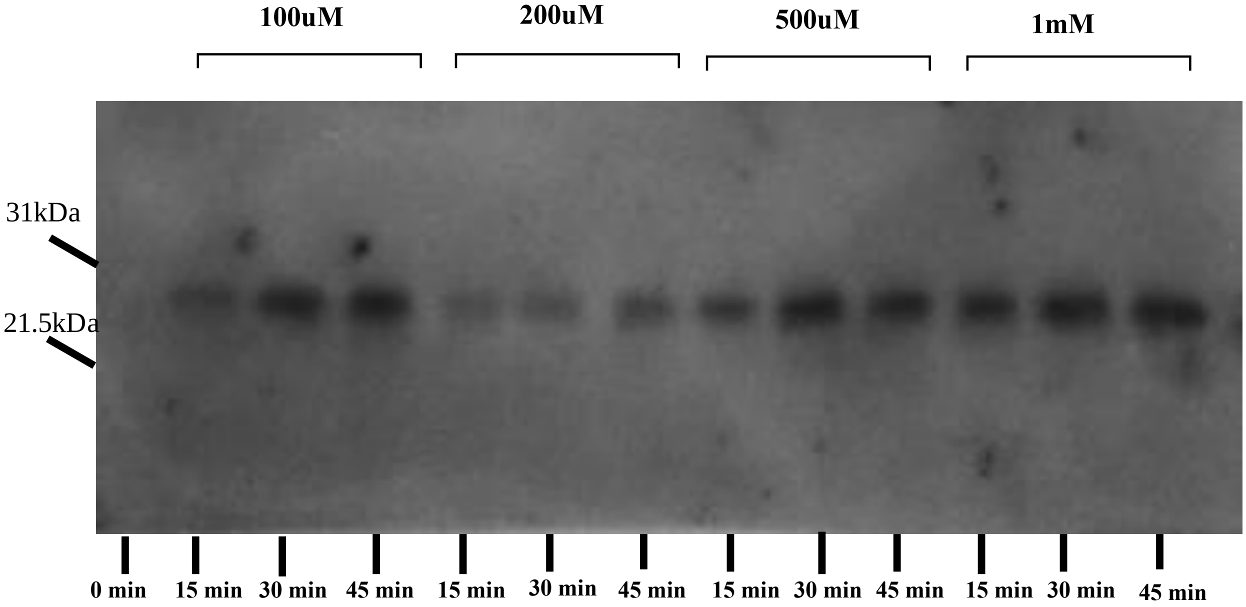
100uM
200uM
500uM
1mM
31kDa
21.5kDa
0 min
15 min
30 min
45 min
15 min
30 min
45 min
15 min
30 min
45 min
15 min
30 min
45 min

Figure 3.8: Western blot probing with streptavidin-HRP for YFP-G_5YYK_{biotin} using Liu's *S.aureus* SrtA. G_5YYK_{biotin} was titrated at the given concentrations and time points were taken at 15, 30, and 45 minutes.

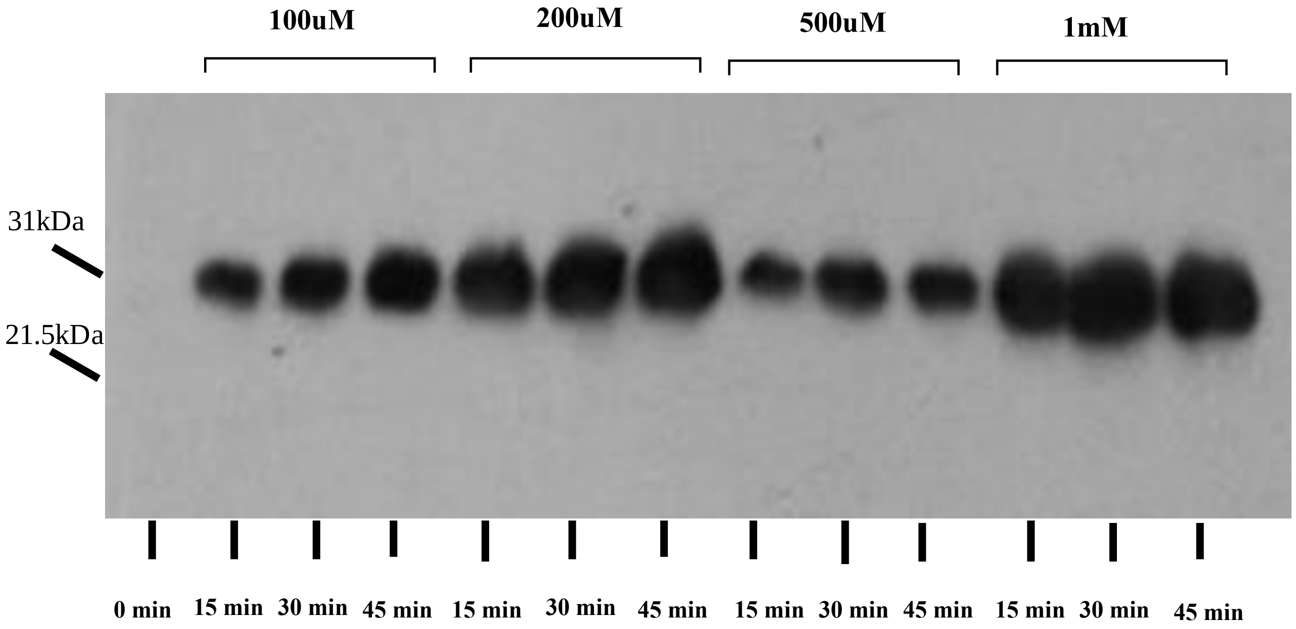
100uM
200uM
500uM
1mM
31kDa
21.5kDa
0 min
15 min
30 min
45 min
15 min
30 min
45 min
15 min
30 min
45 min
15 min
30 min
45 min

Figure 3.9: Western blot probing with streptavidin-HRP for YFP-G_5YYK_{biotin} using Muna's *S.aureus* SrtA. G_5YYK_{biotin} was titrated at the given concentrations and time points were taken at 15, 30, and 45 minutes.

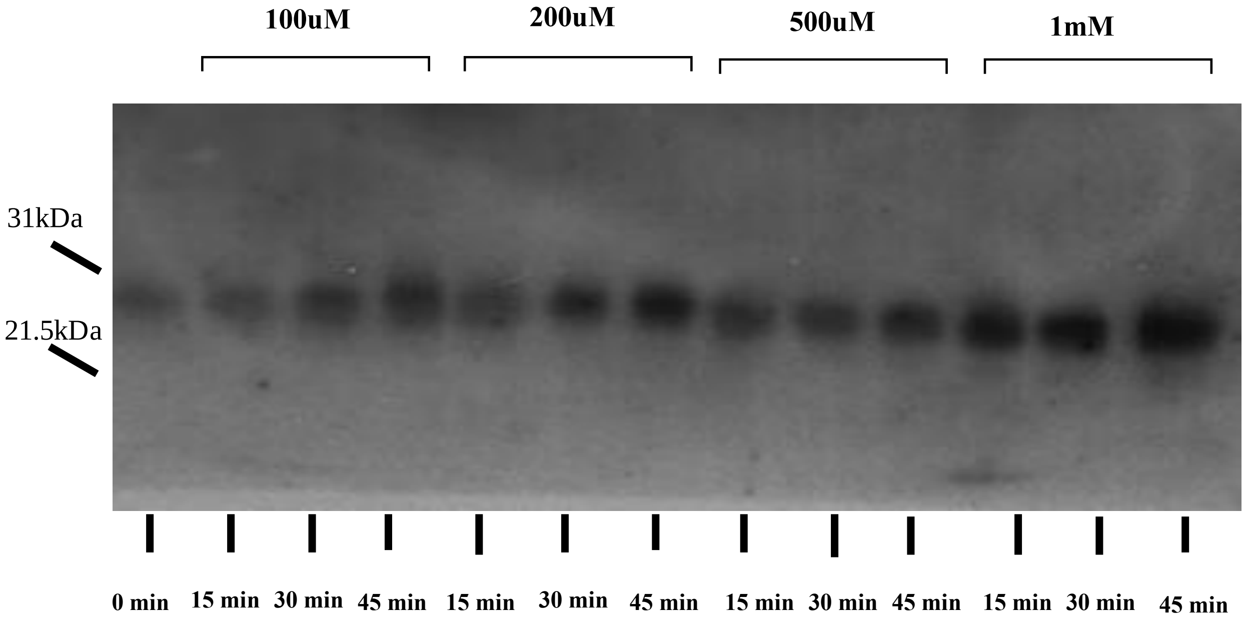
100uM
200uM
500uM
1mM
31kDa
21.5kDa
0 min
15 min
30 min
45 min
15 min
30 min
45 min
15 min
30 min
45 min
15 min
30 min
45 min

Figure 3.10: Liu's *S.aureus* SrtA appears to have a lower pentaglycine K_m than Muna's or WT *S.aureus* SrtA. WT *S.aureus* SrtA kinetic data is shown in blue while Muna's *S.aureus* SrtA and Liu's *S.aureus* SrtA kinetic data are shown in red and green respectively.

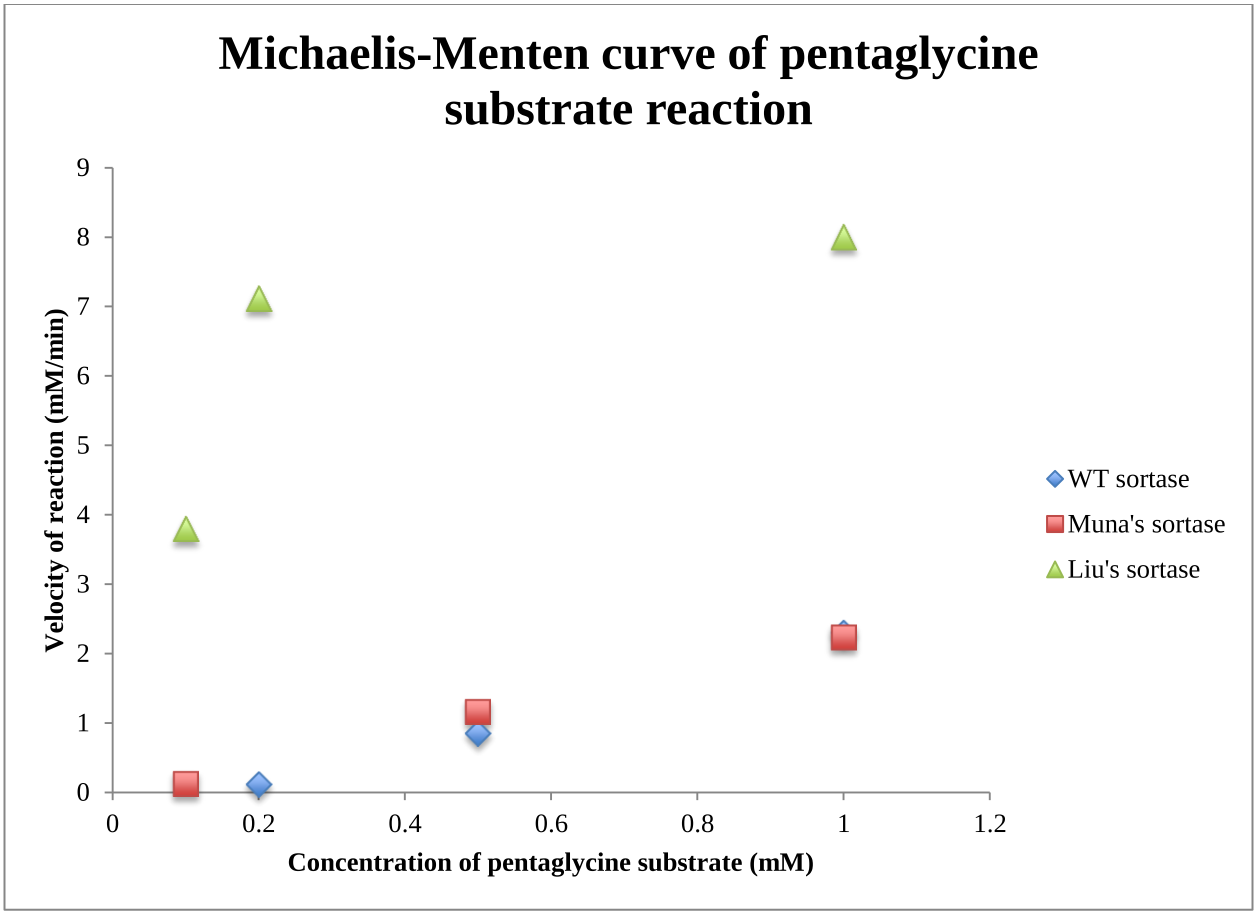
Michaelis-Menten curve of pentaglycine substrate reaction
Velocity of reaction (mM/min)
9
8
7
6
5
4
3
2
1
0
0
0.2
0.4
0.6
0.8
1
1.2
Concentration of pentaglycine substrate (mM)
WT sortase
Muna's sortase
Liu's sortase

Chapter 4

Conclusions

SrtA has been known to be an effective molecular stapler for quite some time, but the catalytic mechanism has eluded researchers. In 2004, the crystal structure of *S.aureus* SrtA was solved with and without its signal peptide, LPETG. The "catalytically active" form of the enzyme shows the peptide approximately 8Å away from the active site, and the active site residues (His120 and Cys184) approximately 5Å away from each other. These problems lead researchers to question the crystal structure since the enzyme does not seem to be in a catalytically active form (Figure 1.6). In 2009, an NMR structure was published which displayed a completely different model for catalysis. In this model, a disulfide bond was used to trap the LPETG substrate as a mimic for the thioacyl intermediate. A bulky head group was also left on the peptide posing steric complications that lead investigators to question how the peptide occupies the active-site pocket. Although there are problems with this structure, it still displays functionally relevant characteristics. In this model, the peptide is closer to the active site and the active site residues are in the right conformation for catalysis (Figure 1.7). The NMR structure is currently thought to be the correct model for SrtA catalysis, but the model does not explain how the substrate gets to the active site. We propose that the crystal structure is not incorrect, but it, in fact, describes an early binding event of the LPXTG substrate while the NMR model represents a later conformation of LPXTG as it approaches the active site. As the sorting signal travels to the active site, the β6/β7 loop moves 10Å to act as a lid, both pushing and closing, on top of the substrate as it moves down a "hydrophobic slide" to the active site in order to undergo catalysis.

Because of SrtA’s utility as a molecular stapler and its low catalytic efficiency, several attempts have been made to utilize directed evolution to make the enzyme more effective. We were able to generate a mutant (Figure 4.1), which increased the catalytic efficiency 10-fold in comparison to WT *S.aureus* SrtA (Table 4.1). Simultaneously, Chen et.al published a mutant (Figure 4.2) that increased the catalytic efficiency of *S.aureus* SrtA 100-fold (Table 4.1). Our mutations seem to map around the substrate binding pocket, but, interestingly, none of the mutations on Chen et. al’s mutant or our mutant directly interact with the substrate leading us to postulate that the mutations help to facilitate the “hydrophobic slide” in some way.

To test this hypothesis, we attempted to crystallize WT *S.aureus* SrtA, Muna’s *S.aureus* SrtA and Liu’s *S.aureus* SrtA to endeavor to understand what made the mutants more catalytically active. Although we were able to purify all of the mutants and *S.aureus* SrtA (Figure 3.1), crystals did not grow so no structural information could be inferred.

Interestingly, we noticed that some mutations we observed in our mutant were seen in other strains of SrtA (specifically the G167E and Q172H mutations). This observation led us to consider the possibility that other strains of SrtA were more “evolved.” Therefore, crystallizing these other strains might bring more insight into SrtA’s mechanism. Several strains were chosen based on their sequence homology to *S.aureus* SrtA (Figure 4.3) with *S.carnosus* SrtA having the closest sequence homology to *S.aureus* SrtA and *L.bacterium* SrtA being the most distinct from *S.aureus* SrtA. We were able to obtain a structure for *G.morbillorum* SrtA, and found that the β6/β7 loop closes over the active site pocket more effectively in the apo-form in comparison to apo *S.aureus* SrtA `. From this, we postulate that the *G.morbillorum* SrtA structure is more effective as a molecular stapler due to the more defined pocket formed by the β6/β7 loop. However, kinetic studies need to be done to confirm this assertion.

There are two components of the SrtA transpeptidase reaction; the first component is the cleavage of the amide bond between the threonine and glycine in the seed sequence while the second component consists of the pentaglycine nucleophile resolving the enzyme-substrate intermediate. We have obtained kinetic data for the first component of the reaction, but elucidating the kinetic parameters of the second component has been problematic. We developed an assay that works under the assumption that the first step of the reaction (acylation) is negligible since the substrate is at a significant enough concentration past the K_m and product formation is monitored via streptavidin-HRP (Figure 4.4). With the aid of this assay, we obtained data that indicates Liu's *S.aureus* SrtA mutant has the lowest pentaglycine K_m in comparison to both WT *S.aureus* SrtA and Muna's *S.aureus* SrtA (Figure 3.10), but Chen et.al reported that the pentaglycine K_m for Liu's *S.aureus* SrtA was 2.9 ± .2 mM which was significantly larger than their reported value for WT *S.aureus* SrtA (140 ± 30 μM). The discrepancy in the kinetic data can be explained by the types of assays that were used since Chen et. al used a HPLC assay to monitor product formation while we used a biotin-labeled peptide and monitored the reaction via streptavidin-HRP.

Unfortunately, we are not close to the LPETG K_m for Muna's *S.aureus* SrtA and WT *S.aureus* SrtA since both of them have a K_m in the mM range (Table 4.1). To approach the LPETG K_m would require very large amounts of the YPF-LPETG substrate, which lead us to generate peptides for a HPLC assay in order to determine the kinetics of the pentaglycine substrate. For this assay, YYALPETGE and GGGGGYYK will be made and the reaction will be monitored via reverse phase HPLC.

In order to test our “hydrophobic slide” hypothesis, we will attempt trap the thio-acyl intermediate through sodium borohydride with a LPXTG peptide and characterize the complex via crystallography for all of the *S.aureus* SrtA mutants as well as the other SrtA strains. This method does not pose the same problems as disulfide trapping, but the sodium borohydride reaction produces hydrogen gas, which is very damaging to proteins. Furthermore, only two crystal structures have been published that isolate the thioacyl intermediate through sodium borohydride trapping which does not leave a solid precedence (Elena Mossessova et.al, 2000). If trapping is not possible, then single molecule FRET will be employed to assess the 10Å movement that occurs in the β6/β7 loop during catalysis (Rahul Roy et. al, 2008).

Finalizing the structural studies on SrtA will help us and the scientific community understand the utility of this enzyme. With this understanding, we can hopefully comprehend ways to manipulate SrtA into being more useful for our needs as a molecular stapler. Since SrtA is an important therapeutic target, understanding the novel mechanism that it uses will be essential to generating antibiotics that attack deadly strains of Gram-positive bacteria such as Methicillin-resistant *Staphylococcus aureus* (MRSA).

Figure 4.1: All of Muna's mutations to *S.aureus* SrtA map around the substrate binding pocket. Muna's mutations of *S.aureus* SrtA. The overall structure of the enzyme is shown in cyan while the mutated residues are shown in red with labels illustrating what the residue was mutated to. The LPETG peptide is colored orange.

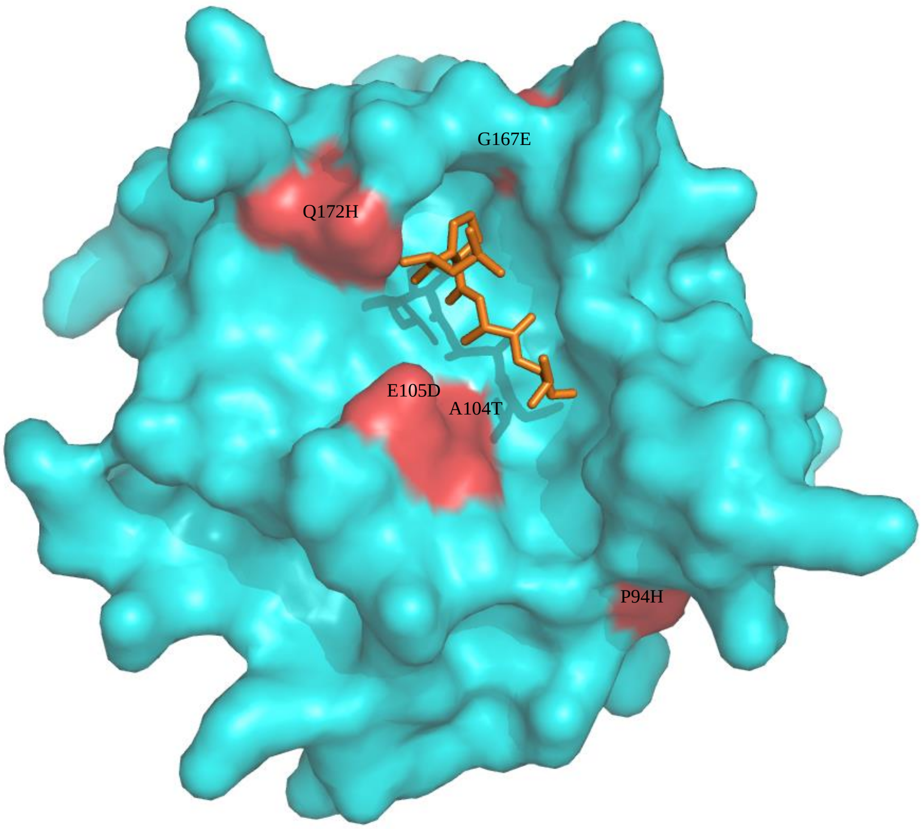
G167E
Q172H
E105D
A104T
P94H

Figure 4.2: The benefit of Liu's mutations to *S.aureus* SrtA is not clear. The overall structure of the enzyme is shown in cyan and the mutated residues are labeled and shown in red. Another view of the enzyme is shown to more clearly display the mutated residues. The LPETG peptide is colored orange.

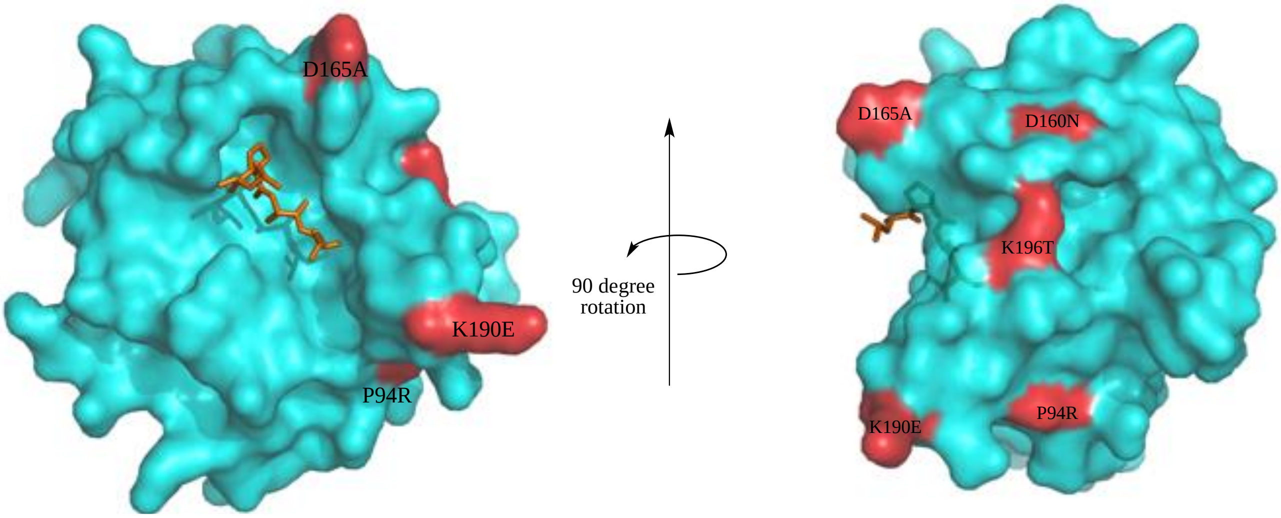
D165A
K190E
P94R
90 degree
rotation
D165A
D160N
K196T
K190E
P94R

Figure 4.3: A Basic Local Alignment Search Tool (BLAST) sequence alignment of *S.aureus* SrtA, *S.carnosus* SrtA, *G.moribillorum* SrtA, *L.mali* SrtA, and *L.bacterium* SrtA. The conserved residues are highlighted in blue and the three catalytic residues have a magenta star over them.

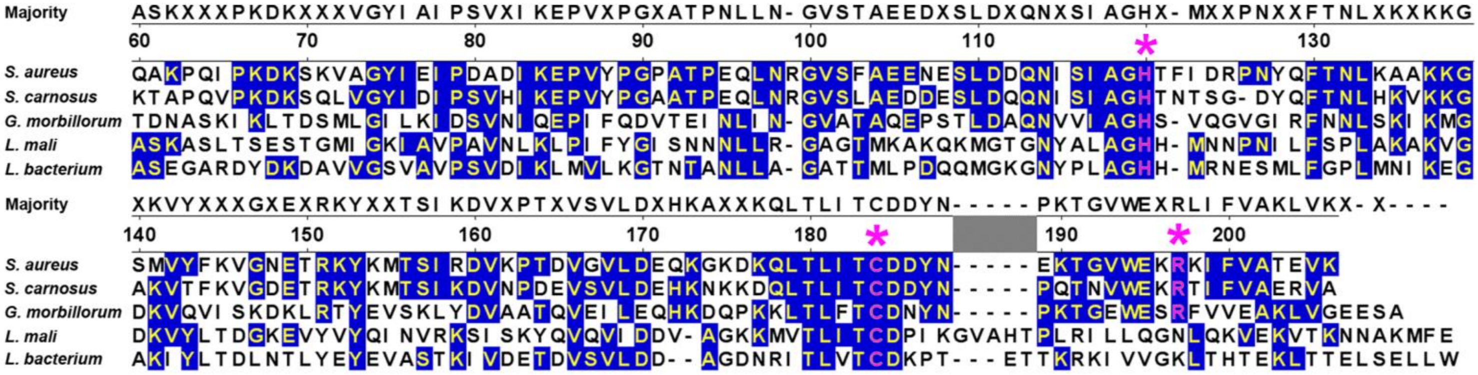

```
Majority        ASKXXXPKDKXXXXVGYIAIPSVXIKEPVXPGXATPNLLN-GVSTAEEDXSLDXQNXSIAGHX-MXXPNXXFTNLXKXKKG
S. aureus       QAKPQIPKDKSKVAGYIEIPDADIKEPVYPGPATPEQLNRGVSFAEENESLDDQNISIAGHTFIDRPNYQFTNLKAAKKG
S. carnosus     KTAPQVPKDKSQLVGYIDIPSVHIKEPVYPGAATPEQLNRGVSLAEDDESLDQQNISIAGHTNTSG-DYQFTNLHKVKKG
G. morbillorum  TDNASKIKLTDSMLGILKIDSVNIQEPIFQDVTEINLIN-GVATAQEPSTLDAQNVVIAGHS-VQGVGIRFNNLSKIKMG
L. mali         ASKASLTSESTGMIGKIAVPAVNLKLPIFYGISNNNLLR-GAGTMKAKQKMGTGNYALAGHH-MNNPNILFSPLAKAKVG
L. bacterium    ASEGARDYDKDAVVGSVAVPSVDIKLMVLKGTNTANLLA-GATTMLPDQQMGKGNYPLAGHH-MRNESMLFGPLMNIKEG

Majority        XKVYXXXGXEXRKYXXTSIKDVXPTXVSVLDXHKAXXKQLTLITCDDYN-----PKTGVWEXRLIFVAKLVKX-X----
S. aureus       SMVYFKVGNETRKYKMTSIRDVKPTDVGVLDEQKGKDKQLTLITCDDYN-----EKTGVWEKRKIFVATEVK
S. carnosus     AKVTFKVGDETRKYKMTSIKDVNPDEVSVLDEHKNKKDQLTLITCDDYN-----PQTNVWEKRTIFVAERVA
G. morbillorum  DKVQVISKDKLRTYEVSKLYDVAATQVEILEQHKDQPKKLTLFTCDNYN-----PKTGEWESRFVVEAKLVGEESA
L. mali         DKVYLTDGKEVYVYQINVRKSISKYQVQVIDDV-AGKKMVTLITCDPIKGVAHTPLRILLQGNLQKVEKVTKNNAKMFE
L. bacterium    AKIYLTDLNTLYEYEVASTKIVDETDVSVLDD--AGDNRITLVTCDKPT---ETTKRKIVVGKLTHTEKLTTELSELLW
```

Figure 4.4: Diagram of the pentaglycine assay. Saturating amounts of YFP-LPXTG are added so that the acylation step is negligible while G_5YYK_{biotin} is varied. YFP-$LPXTGG_5YYK_{biotin}$ product formation is monitored via streptavidin-HRP.

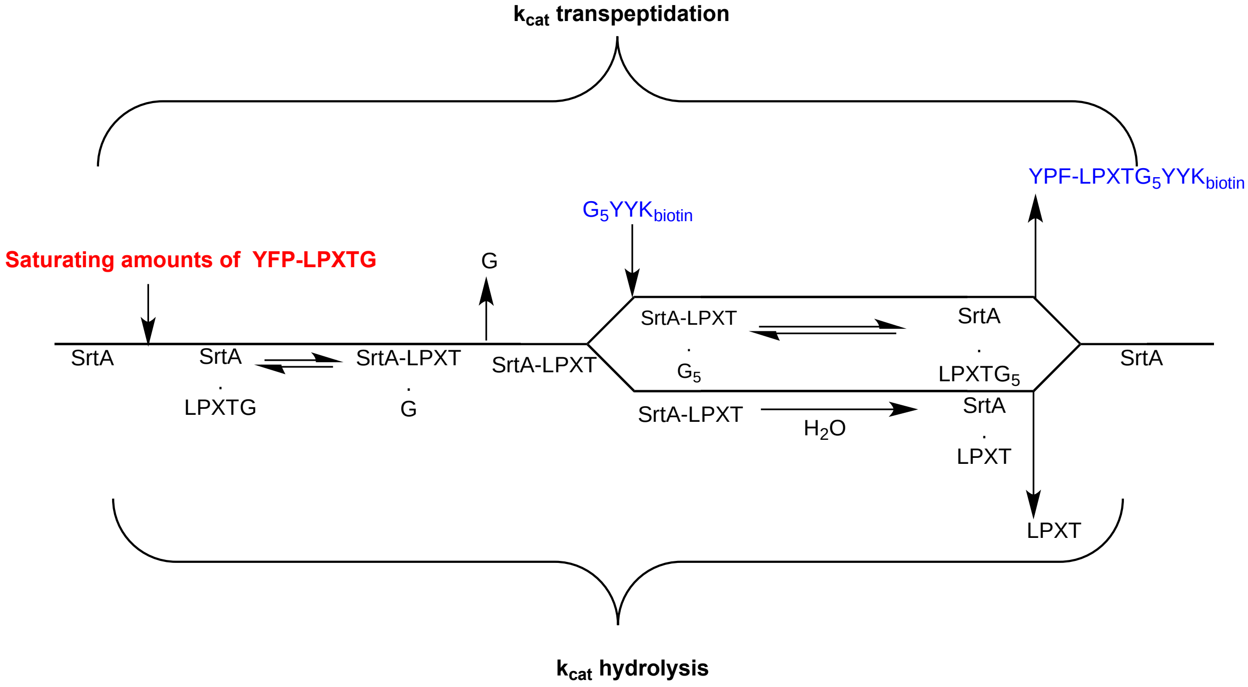
k$_{cat}$ transpeptidation
Saturating amounts of YFP-LPXTG
G
G$_5$YYK$_{biotin}$
YPF-LPXTG$_5$YYK$_{biotin}$
SrtA
SrtA · LPXTG
SrtA-LPXT · G
SrtA-LPXT
SrtA-LPXT · G$_5$
SrtA · LPXTG$_5$
SrtA
SrtA-LPXT
H$_2$O
SrtA · LPXT
LPXT
k$_{cat}$ hydrolysis

Table 4.1: Kinetic parameters for the acylation step of *S.aureus* SrtA and its mutants. All reactions were done at 23^{o}C and a DABSYL-EDANS peptide (Anaspec) was used to monitor the reaction via fluorescence at 493nm.

Sortase A	kcat (s-1)	Km (mM)	kcat/Km (M-1s-1)
WT *S.aureus* SrtA	1.3 ± 0.1	8.1± 0.3	150± 20
Muna's *S.aureus* SrtA	3.15± 0.3	1.6± 0.5	2000± 100
Liu's *S.aureus* SrtA	5.4± 0.4	.23± 0.02	23000± 3000

Literature cited

Bentley, M. L., Lamb, E. C., & McCafferty, D. G. (2008). Mutagenesis studies of substrate recognition and catalysis in the sortase A transpeptidase from Staphylococcus aureus. *The Journal of Biological Chemistry*, *283*(21), 14762–14771.

Chang, T. K., Jackson, D. Y., Burnier, J. P., & Wells, J. A. (1994). Subtiligase: a tool for semisynthesis of proteins. *Proceedings of the National Academy of Sciences of the United States of America*, *91*(26), 12544–8.

Chen, I., Dorr, B. M., & Liu, D. R. (2011). A general strategy for the evolution of bond-forming enzymes using yeast display. *Proceedings of the National Academy of Sciences of the United States of America*, *108*(28), 11399–11404.

Frankel, B. a, Kruger, R. G., Robinson, D. E., Kelleher, N. L., & McCafferty, D. G. (2005). Staphylococcus aureus sortase transpeptidase SrtA: insight into the kinetic mechanism and evidence for a reverse protonation catalytic mechanism. *Biochemistry*, *44*(33), 11188–11200.

Hendrickx, A. P. a, Budzik, J. M., Oh, S.-Y., & Schneewind, O. (2011). Architects at the bacterial surface - sortases and the assembly of pili with isopeptide bonds. *Nature Reviews Microbiology*, *9*(3), 166–176.

Ilangovan, U., Ton-That, H., Iwahara, J., Schneewind, O., & Clubb, R. T. (2001). Structure of sortase, the transpeptidase that anchors proteins to the cell wall of Staphylococcus aureus. *Proceedings of the National Academy of Sciences of the United States of America*, *98*(11), 6056–61.

Jackson, D. Y., Burnier, J., Quan, C., Stanley, M., Tom, J., & Wells, J. a. (1994). A designed peptide ligase for total synthesis of ribonuclease A with unnatural catalytic residues. *Science*, *266*(5183), 243–247.

Kast, P., & Hilvert, D. (1997). 3D structural information as a guide to protein engineering using genetic selection. *Current opinion in structural biology*, *7*(4), 470–9.

Kazlauskas, R. J., & Bornscheuer, U. T. (2009). Finding better protein engineering strategies. *Nature Chemical Biology*, *5*(8), 526–9.

Kim, Y.W., Grossmann, T. N., & Verdine, G. L. (2011). Synthesis of all-hydrocarbon stapled α-helical peptides by ring-closing olefin metathesis. *Nature Protocols*, *6*(6), 761–771.

Lee, D., Redfern, O., & Orengo, C. (2007). Predicting protein function from sequence and structure. *Nature Reviews Molecular Cell Biology*, *8*(12), 995–1005.

Maresso, A. W., & Schneewind, O. (2008). Sortase as a target of anti-infective therapy. *Pharmacological Reviews*, *60*(1), 128–141.

Mossessova, E., & Lima, C. D. (2000). Ulp1-SUMO crystal structure and genetic analysis reveal conserved interactions and a regulatory element essential for cell growth in yeast. *Molecular Cell*, *5*(5), 865–876.

Naik, M. T., Suree, N., Ilangovan, U., Liew, C. K., Thieu, W., Campbell, D. O., Clemens, J. J., et al. (2006). Staphylococcus aureus Sortase A transpeptidase. Calcium promotes sorting signal binding by altering the mobility and structure of an active site loop. *The Journal of Biological Chemistry*, *281*(3), 1817–1826.

Ollivier, N., Dheur, J., Mhidia, R., Blanpain, A., & Melnyk, O. (2010). Bis(2-sulfanylethyl)amino native peptide ligation. *Organic letters*, *12*(22), 5238–41.

Roy, R., Hohng, S., & Ha, T. (2008). A practical guide to single-molecule FRET. *Nature methods*, *5*(6), 507–16.

Studier, F. W. (2005). Protein production by auto-induction in high-density shaking cultures. *Protein Expression and Purification*, *41*(1), 207–234.

Suree, N., Liew, C. K., Villareal, V. a, Thieu, W., Fadeev, E. a, Clemens, J. J., Jung, M. E., et al. (2009). The Structure of the Staphylococcus aureus Sortase-Substrate Complex Reveals How the Universally Conserved LPXTG Sorting Signal Is Recognized. *The Journal of Biological Chemistry*, *284*(36), 24465–24477.

Tian, B.-X., & Eriksson, L. a. (2011). Catalytic Mechanism and Roles of Arg197 and Thr183 in the Staphylococcus aureus Sortase A Enzyme. *The Journal of Physical Chemistry B*, *115*(44), 13003–11.

Ton-That, H., Mazmanian, S. K., Alksne, L., & Schneewind, O. (2002). Anchoring of surface proteins to the cell wall of Staphylococcus aureus. Cysteine 184 and histidine 120 of sortase form a thiolate-imidazolium ion pair for catalysis. *The Journal of Biological Chemistry*, *277*(9), 7447–7452.

Whisstock, J. C., & Lesk, A. M. (2003). Prediction of protein function from protein sequence and structure. *Quarterly Reviews of Biophysics*, *36*(3), 307–340.

Yamamura, Y., Hirakawa, H., Yamaguchi, S., & Nagamune, T. (2011). Enhancement of sortase A-mediated protein ligation by inducing a β-hairpin structure around the ligation site. *Chemical Communications*, *47*(16), 4742–4744.

Zong, Y., Bice, T. W., Ton-That, H., Schneewind, O., & Narayana, S. V. L. (2004). Crystal structures of Staphylococcus aureus sortase A and its substrate complex. *The Journal of Biological Chemistry*, *279*(30), 31383–31389.